

**Contract No:**

This document was prepared in conjunction with work accomplished under Contract No. DE-AC09-08SR22470 with the U.S. Department of Energy (DOE) Office of Environmental Management (EM).

**Disclaimer:**

This work was prepared under an agreement with and funded by the U.S. Government. Neither the U. S. Government or its employees, nor any of its contractors, subcontractors or their employees, makes any express or implied:

- 1 ) warranty or assumes any legal liability for the accuracy, completeness, or for the use or results of such use of any information, product, or process disclosed; or
- 2 ) representation that such use or results of such use would not infringe privately owned rights; or
- 3) endorsement or recommendation of any specifically identified commercial product, process, or service.

Any views and opinions of authors expressed in this work do not necessarily state or reflect those of the United States Government, or its contractors, or subcontractors.

We put science to work.™



**Savannah River  
National Laboratory®**

OPERATED BY SAVANNAH RIVER NUCLEAR SOLUTIONS

A U.S. DEPARTMENT OF ENERGY NATIONAL LABORATORY • SAVANNAH RIVER SITE • AIKEN, SC

# Stainless Steel Corrosion during H-Canyon Resin Digestion

E. A. Kyser

J. I. Mickalonis

October 2018

SRNL-STI-2018-00603

SRNL.DOE.GOV

## **DISCLAIMER**

This work was prepared under an agreement with and funded by the U.S. Government. Neither the U.S. Government or its employees, nor any of its contractors, subcontractors or their employees, makes any express or implied:

- warranty or assumes any legal liability for the accuracy, completeness, or for the use or results of such use of any information, product, or process disclosed; or
- representation that such use or results of such use would not infringe privately owned rights; or
- endorsement or recommendation of any specifically identified commercial product, process, or service.

Any views and opinions of authors expressed in this work do not necessarily state or reflect those of the United States Government, or its contractors, or subcontractors.

**Printed in the United States of America**

**Prepared for  
U.S. Department of Energy**

**Keywords:** Reillex HPQ, Resin Digestion,  
H-Canyon, Plutonium, Permanganate,  
Corrosion

**Retention:** *Permanent*

## Stainless Steel Corrosion during H-Canyon Resin Digestion

E. A. Kyser  
J. I. Mickalonis

October 2018

---

Prepared for the U.S. Department of Energy under  
contract number DE-AC09-08SR22470.



## REVIEWS AND APPROVALS

### AUTHORS:

*original approved by E. A. Kyser 11/5/2018*

---

E. A. Kyser, Separations and Actinide Science Programs	Date
--	------

*original approved by J.I. Mickalonis 11/5/2018*

---

J. I. Mickalonis, Corrosion and Material Performance	Date
--	------

### TECHNICAL REVIEWERS:

*original approved by J. M. Duffey 11/5/2018*

---

Jon Duffey, Separations and Actinide Science Programs	Date
---	------

*original approved by Rod E. Fuentes 11/5/2018*

---

R. E. Fuentes, Corrosion and Material Performance	Date
---	------

### APPROVALS:

*original approved by Tim Brown 11/5/2018*

---

Timothy Brown, Manager Separations and Actinide Science Programs	Date
---	------

*original approved by Samuel D. Fink 11/5/2018*

---

S. D. Fink, Director Chemical Process Technology	Date
---	------

*original approved by B. J. Wiersma 11/5/2018*

---

Bruce Wiersma, Manager Corrosion and Material Performance	Date
--	------

*original approved by Kristine E. Zeigler 11/5/2018*

---

Kristine, E. Zeigler, Director Materials Science and Technology	Date
--	------

*Approved per Email for James Therrell by E. A. Kyser 11/5/2018*

---

James Therrell, Manager H-Canyon Engineering	Date
---	------

## **PREFACE OR ACKNOWLEDGEMENTS**

The authors wish to acknowledge the assistance of T. H. Murphy, and S. A. Crossland during the corrosion assessment of the test coupons.

## EXECUTIVE SUMMARY

Historically HB-Line has transferred a slurry of used anion exchange resin to the H-Canyon Tank 5.2 where caustic digestion using permanganate was performed prior to transfer to the tank farm. Recent digestions had switched to an acid flowsheet. During recent testing to investigate the hydrogen generation rate (HGR) for the resin acid digestion process, the experimental apparatus fabricated from stainless steel and nickel-chromium alloys was found to have suffered significant localized corrosion which failed a heating rod. This observed corrosion raised concerns about the integrity of Tank 5.2, which is fabricated of 304L stainless steel. An exploratory study was undertaken to better understand the cause of this corrosion as well as during a caustic digestion and to use these data to assess the viability of Tank 5.2 using the current acid digestion flowsheet versus the previous caustic flowsheet.

The study was conducted with both chloride form resin, which was used in the HGR experiment, and nitrate form resin, which is the type used in HB-line. The testing results with both forms of resin in an acid digestion demonstrated that the primary mode of corrosion was intergranular attack (IGA) due to the highly oxidizing conditions of the digestion: high molar nitric acid (8M), presence of an oxidizing species (permanganate), and elevated temperatures (76 °C). The presence of chloride in the digestion solution from using the chloride form resin did not appear to measurably contribute to the observed corrosion and may at best have a secondary effect of accelerating depths of attack. These results differed from those observed for the HGR test vessel which may be attributed to differences in experimental technique, including test times, gas flow, and material sources. In this exploratory study, sufficient data was not acquired to further delineate the impact of chloride on localized corrosion (such as pitting). The presence of chloride in the digestion solution also had no impact on the general corrosion rate. Neutral pH digestion of the nitrate form resin was shown to cause negligible damage to stainless steel.

In the testing, the test coupons were exposed to evaluate the degree of corrosion in the vapor space, immersed in the digestion solution, and at the air/liquid interface. Welded and non-welded coupons were tested. The degree of IGA varied with the exposure location as well as the presence of welding. General corrosion rates were measured at approximately 90 mpy. The greatest corrosion was observed at the air/liquid interface with the maximum depth of penetration measured at 8 mils, which is attributed to the IGA and grain dropping.

As based on the current testing, the current material condition of Tank 5.2 is expected to have suffered IGA from the two previous acid digestions on the liquid-exposed surface with the greatest corrosion along the air/liquid interface. Previous caustic digestions are not expected to have caused corrosion of the coil or tank walls. As based on the maximum depth of penetration (0.008 inch) measured during this testing, the Tank 5.2 coil and wall thickness would have lost a total of 0.016 inch for two digestions. Doubling this depth of penetration as a safety margin would yield a total wall loss of 0.032 inch. This approach accounts for loss equivalent to the deepest depth of penetration on test coupons and allows for the impact of variables such as high temperatures at the heating coil surfaces. Since localized spots of grain drop out occurred on liquid-exposed surfaces, the two proposed acid digestions could still cause a total wall loss of 0.064 inch, consuming the total corrosion allowance, but without compromising the containment function of the tank and coils. While Tank 5.2 is expected to withstand two additional acid digestions, a condition assessment of the tank, i.e. a visual examination or coil pressure testing, would provide valuable data on Tank 5.2 utility, especially at the end of any additional digestions.

## TABLE OF CONTENTS

LIST OF TABLES .....	viii
LIST OF FIGURES .....	viii
LIST OF ABBREVIATIONS.....	x
1.0 Introduction.....	11
2.0 Experimental Procedure.....	11
2.1 Quality Assurance .....	13
3.0 Results and Discussion .....	14
3.1 Observations on Test 1 Reillex HPQ Batch 1364.1 chloride form resin.....	14
3.2 Observations on Test 2 Reillex HPQ HB-Line nitrate form resin sample .....	15
3.3 Observations on Test 2a Reillex HPQ HB-Line resin sample (Nitrate form resin) .....	17
3.4 Observations on Test 3 Reillex HPQ HB-Line resin sample (nitrate form resin) Neutral pH .....	20
3.5 Corrosion Assessment of Test Coupons.....	21
3.5.1 General Corrosion Rate .....	22
3.5.2 Localized Corrosion Observations – Tests 1, 2, and 3 .....	24
3.5.3 Test 2a Results .....	31
4.0 Implications of Testing .....	34
5.0 Conclusions.....	36

## LIST OF TABLES

Table 2-1. Standard Experimental Recipe .....	12
Table 2-2. Modified Test Plan .....	13
Table 3-1. Corrosion Coupon Weight Loss .....	23
Table 3-2 Localized Corrosion Observation Summary from Corrosion Testing of Acidic Resin Digestion Process .....	33

## LIST OF FIGURES

Figure 2-1. Equipment configuration.....	12
Figure 3-1. Coupon appearance at the end of a 15-h acidic digestion - Test 1 chloride form resin. ....	14
Figure 3-2. Coupons from Test 1 after cleanup. (from left to right) vapor, interface, submerged welded coupons, and non-welded coupon at the interface. Black arrow denotes area with accelerated corrosion near position of uncoated hanger wire.....	14
Figure 3-3. Coupon appearance raised above beaker in Test 2 nitrate form resin. Note purple color from permanganate is absent in 15-h photo. ....	16
Figure 3-4. Coupon location relative to solution level 14.5 h into Test 2.....	16
Figure 3-5. Test 2 cleanup showing MnO <sub>2</sub> coating on beaker and coupon #05. ....	17
Figure 3-6. Coupons from Test 2 after cleanup: (from left to right) welded vapor, welded interface, welded immersed, and non-welded interface. Staining is prevalent on the coupons.....	17
Figure 3-7. Start of Test 2a .....	18
Figure 3-8. Appearance of coupons: 30 min into Test 2a.....	18
Figure 3-9. Appearance of coupons: 3 h into Test 2a. ....	18
Figure 3-10. Appearance of coupons: 5 h into Test 2a. ....	19
Figure 3-11. Coupons before and after caustic adjustment.....	19
Figure 3-12. Corrosion coupons from Test 2a after cleaning. (304W #124 exposed to both Test 2 and 2a, 304W #124 and #52 exposed through neutralization step, 304W #54 removed prior to neutralization step) .....	19
Figure 3-13. Position of coupons in solution Test 3. ....	20
Figure 3-14. Coupon cleanup.....	20
Figure 3-15. Nitrous acid cleaning- Coupon 304L #05. ....	21
Figure 3-16. Test 3 Pre- and post-test appearance of coupons. ....	21

Figure 3-17. Vapor-exposed coupons from Tests 1 (#160, acid digestion) and 3 (#184, neutral pH digestion) using nitrate form resin.....	24
Figure 3-18 Liquid-exposed coupons from Test 1 (left, acid digestion) and Test 2 (middle, acid digestion) and the vertical interfacial coupon from Test 3 (right, neutral pH digestion). .....	25
Figure 3-19 Micrographs (200x) showing the intergranular attack observed on the immersed coupon from Test 1 using the chloride form resin acid digestion.....	25
Figure 3-20. Micrograph (100x) of immersed 304W coupon (#148) after a 15-hour acid digestion of the nitrate form resin at 76 °C (Test 2) showing IGA on the surface along with an area of grain drop out; line profile through area of grain drop out.....	26
Figure 3-21. Test coupons from Test 3 after 15 hours of the nitrate form resin neutral pH digestion performed at 76 °C; coupons are shown in the following order: 304W vapor-exposed only, 304W interfacial exposure, 304W liquid-exposed only (not cleaned in nitrous acid), 304L interfacial exposure. ....	26
Figure 3-22 Interfacial 304W coupons after resin digestion tests with: (left) Test 1- acid digestion, chloride form resin; (middle) Test 2 - acid digestion, nitrate form resin; and (right) Test 3 - neutral pH digestion, nitrate form resin .....	27
Figure 3-23. Interfacial region from 304W coupon after 15-hour acid digestion at 76 °C of chloride form resin (Test 1).....	27
Figure 3-24. Interfacial region near the weld from 304W coupon after 15-hour acid digestion at 76 °C of nitrate form resin; weld is the upper half of micrograph and height scan (Test 2).....	28
Figure 3-25. The corrosion morphology of the vapor and liquid portions of the Test 1 304L coupon .....	28
Figure 3-26.. Micrographs (100x) of the air/liquid interface 304L coupon (#05) from nitrate form resin acid digestion test after 15 hours at 76 °C (Test 2) .....	29
Figure 3-27. Sectioned interfacial 304L coupon from Tests 1 (left) and 2 (right); missing section was mounted for cross-sectional examination. ....	30
Figure 3-28. Micrographs (500x) showing attack of the air/liquid interface 304L coupon (#10) from chloride form resin acid digestion test after 15 hours at 76 °C (Test 1).....	30
Figure 3-29. Micrograph montage (200x) showing attack in the interfacial region of the air/liquid interface 304L coupon (#10) from chloride form resin acid digestion test after 15 hours at 76 °C (Test 1).....	31
Figure 3-30. Micrographs (500x) of the unetched and etched cross section of an interfacial portion of 304L coupon (#05) from nitrate form resin acid digestion test after 15 hours at 76 °C (Test 2).....	31
Figure 3-31. Surface corrosion morphology for Coupons #52 and #54 from Test 2a: .....	32
Figure 3-32. Cross section view of interface area for Coupon #124 from Test 2a .....	33

## LIST OF ABBREVIATIONS

h	Hours
HGR	Hydrogen Generation Rate
IGA	Intergranular Attack
LCM	Laser Confocal Microscope
MW	Molecular Weight
M	Molar concentration
n/a	Not applicable
NAA	Neutron Activation Analysis
RTD	Resistance temperature detector
s	Seconds
SRNL	Savannah River National Laboratory
TFE	Tetrafluoroethylene

## 1.0 Introduction

Historically HB-Line has transferred a slurry of used anion exchange resin to H-Canyon Tank 5.2 where it was digested with permanganate prior to transfer to the waste tank farm. Due to concerns with radioactive ruthenium volatilization (and release) during digestion, these digestions were performed after partial neutralization. That risk has not been an issue recently due to the lack of fission products in the materials being processed currently in HB-Line. The digestion flowsheet was developed in the early 1960s by Synder<sup>1</sup> but since that time several documents<sup>2,3,4</sup> have been written on studies about various aspects of the process. In 2009, Kyser<sup>5</sup> revisited issues with pH control<sup>6</sup> of resin digestion and recommended that, rather than risk a digestion failure (from high pH), the resin digestion could be performed under acidic conditions. No experimental evaluation of corrosion was performed at that time. Work by Kranzlein<sup>7</sup> appeared to show that corrosion rates were suppressed by the presence of resin during the digestion. Recently while performing hydrogen generation rate (HGR) testing, Woodham<sup>8</sup> observed significant intergranular attack (IGA) on all metallic surfaces of the experimental apparatus and suspect pitting at the air/liquid interface for the stainless steel test vessel and Alloy 800 heating rod. The current work is an exploratory study prompted by those observations as requested by H-Canyon personnel.<sup>9</sup>

## 2.0 Experimental Procedure

The experimental setup consisted of a 1-L beaker placed on a Thermo Scientific Super Nuova digital stirring hotplate. The solution temperature was controlled using a ¼" Teflon™ coated Type-K thermocouple using the external probe option of the hotplate. The temperature measurement system was cross-checked with a calibrated resistance temperature detector (RTD) probe (Control Company, model 4132, RTD platinum thermometer) at 76 °C with agreement to ±0.5 °C. A custom lid with coupon hanger was fabricated by the SRNL glass shop using a large watchglass and glass rod. Tetrafluoroethylene (TFE) coated copper wire was used to suspend welded and non-welded coupons from the beaker lid (see Figure 2-1 a) and b) for assembly details). A short section of Tygon® tubing was placed on the end of the hanger rod to keep the hanger wires from sliding off the rod when the lid was adjusted. After the first test, it was suspected that corrosion of the end of the hanger wire may have contributed to redox related corrosion. Prior to the second test the ends of the hanger wires were coated in epoxy (Devcon #14250) to protect them from exposure to acid condensation.

---

<sup>1</sup> M. D. Snyder, "Dissolution of Ion Exchange Resins", DP-717, E. I. Du Pont de Nemours & Co, Savannah River Laboratory, Aiken, SC, July 1962.

<sup>2</sup> J. A. Wehner, "Permanganate Dissolution of Macroporous Anion Exchange Resin", DPST-88-569, E. I. Du Pont de Nemours & Co, Savannah River Laboratory, Aiken, SC, May 19, 1988.

<sup>3</sup> B. W. Walker, "Permanganate Degradation of Reillex™ HPQ Ion Exchange Resin for use in HB-Line", WSRC-TR-98-00235, Westinghouse Savannah River Company, Savannah River Technology Center, Aiken, SC, December 21, 1998.

<sup>4</sup> W. J. Crooks, Analysis of Permanganate-Digested Reillex™ HPQ Anion Exchange Resin, WSRC-TR-2001-00326, Westinghouse Savannah River Company, Savannah River Technology Center, Aiken, SC, October 2, 2001.

<sup>5</sup> E.A. Kyser, "Flowsheet Validation for the Permanganate Digestion of Reillex™ HPQ Anion Resin", SRNL-STI-2009-00423, Rev. 0, Savannah River National Laboratory, September 2009.

<sup>6</sup> J. W. Ladbury, C. F. Cullis, "Kinetics and Mechanism of Oxidation by Permanganate", Chemical Reviews, 58, 403 (1958).

<sup>7</sup> P. M. Kranzlein, Corrosion of Stainless Steel in KMnO<sub>4</sub> and HNO<sub>3</sub>-Mn(NO<sub>3</sub>)<sub>2</sub> Solutions", DPST-60-209, Memo to W. J. Mottel, March 16, 1960.

<sup>8</sup> W.H. Woodham, C.J. Martino, "Measurement of Hydrogen Generation Rates during Digestion, Neutralization, Transfer, and Storage of Reillex HPQ Resin", SRNL-STI-2018-00460, Revision 0, Savannah River National Laboratory, October 2018.

<sup>9</sup> W. H. Clifton, "Reillex Resin Digestion", NMMD-HTS-2018-3426, 9/13/2018.



a) Beaker with coupons suspended from hanger      b) Start of Test 1

Figure 2-1. Equipment configuration.

The standard chemical recipe for these tests is shown in Table 2-1 based on past flowsheet work.<sup>5</sup> The chemicals were added in the order shown with  $\text{KMnO}_4$  added as powder and dissolved into water. The negative values of concentration of caustic reflect its use to neutralize the nitric acid.

Table 2-1. Standard Experimental Recipe

Description	Weight	Volume	Acid		Permanganate		Nitrate		MW	Density
	g	mL	mmoles	M	mmoles	M	mmoles	M	g/mole	g/cc
DI H <sub>2</sub> O	351	351								0.9986
KMnO <sub>4</sub>	20				127				158.03	
8M HNO <sub>3</sub>	106	85	680	8			680	8		1.25
Reillex HPQ	2.17	5					20	4		
50 wt % NaOH (Test 3 only)	54	35	-679	-19.4					105.99	1.54
		476		1.4		0.27		1.5		1.09

Table 2-2 shows the Modified Test Plan matrix. Tests 1 and 2 were performed to investigate the effect on stainless steel corrosion of the suspect chloride form resin sample used in the Woodham<sup>8</sup> test compared to a sample of the actual HB-Line nitrate-form resin. After the observations of a significant coating (presumed to be  $\text{MnO}_2$ ) on the coupons in Tests 1 and 2, Test 2a was added to the plan. For Test 2a, the solution was monitored approximately hourly to determine how long the highly-oxidizing permanganate persisted. After 5 hours, the purple color of permanganate was no longer present. One coupon was removed from the test at this point, and the acidic solution was pH adjusted with caustic (50 wt % NaOH) to a pH > 10, making observations on the behavior of the  $\text{MnO}_2$  coating. In addition to assessing the permanganate oxidation, Test 2a was also used to investigate the effect on stainless steel corrosion of cumulative acid digestions by re-exposing a coupon from Test 2. In Test 3 the solution was neutralized with caustic prior to the digestion to reflect the historical alkaline digestion flowsheet for comparison purposes. Adjustments of pH in Tests 2a and 3 were performed with wide range pH paper. Initially Test 4 was proposed to test the effect of purge gas flow (air) on the vapor phase corrosion rate but based on the minimal weight loss results for the vapor phase coupons of Tests 1 and 2, this test was determined not to be necessary after a discussion with the customer.

Table 2-2. Modified Test Plan

Test #	Resin		Vapor Phase	Digestion	pH	T, C		Final pH
1	Reillex HPO Batch 1364.1	Suspect chloride form resin	no purge	Acidic	0	76	15 hr	0
2	Reillex HPO HBL sample	Nitrate form resin	no purge	Acidic	0	76	15 hr	0
2a	Reillex HPO HBL sample	Nitrate form resin	no purge	Acidic	0	76	Monitor hourly,	
							Neutralize at end	>10
3	Reillex HPO HBL sample	Nitrate form resin	no purge	Neutral	4-8	76	15 hr	4-8
4	Reillex HPO HBL sample	Nitrate form resin	Vapor phase purge	Acidic		76	Canceled	

Due to the 15-hour duration of most tests, those experiments were initiated late in the afternoon and the digestion was performed overnight. Water was initially added to the top of the watchglass to enhance condensation within the covered beaker and reduce water loss from the system. but the water evaporated after 3-6 hours. Additional water was not added overnight.

The test coupons were fabricated of 304 and 304L stainless steel. The difference in composition of these alloys is the level of carbon present with 304L containing carbon less than 0.3 wt.% and 304 less than 0.8 wt.%. The 304 coupons were welded (304W) while the 304L coupons were not welded. Careful weighing of the coupons before and after the experiment allowed for calculation of an average general corrosion rate. After testing the coupons were examined using a Laser Confocal Microscope (LCM).

Corrosion coupons were cleaned and dried (with Alconox™ wash, water rinse, ethanol rinse, air blow-dry, and “kimwipe” wrap) prior to testing. After cleaning these coupons, they were only handled with either clean nitrile gloves or cotton glove-liners. Photographs of the coupons were taken prior to each test and throughout the testing and cleanup process. Prior to post-testing characterization, each coupon was initially washed with water and any residual acid was neutralized with a 0.1 M sodium carbonate rinse solution. A dilute nitric acid-sodium nitrite solution was used to dissolve the MnO<sub>2</sub> coating that formed on the coupon surfaces. Neither the nitric acid nor sodium nitrate was measured but the nitric acid was kept dilute (< 0.5M) and small amounts of nitrite were added to make the solution pale blue (indicating the presence of nitrous acid). This condition quickly dissolved the MnO<sub>2</sub> by reducing the Mn(IV) to Mn(II).

Several configurations of coupons were used to evaluate the impact of the exposure condition on stainless steel corrosion. For the Test 1 configuration, all three 304W coupons were suspended horizontally; (in the vapor phase, at the air/liquid interface, and in the liquid phase). The 304L coupon was oriented vertically with the air/liquid interface across the width of the coupon in each test. The configuration for the remaining tests was to suspend the 304W interfacial coupon vertically like the 304L coupon, which exposed significant area in all three exposure conditions. Coupons located at the interface (whether oriented horizontally or vertically) resulted in weight loss (and eventually corrosion rates) that reflect the multiple exposure conditions (and thus are averaged results). Tests 1, 2 and 3 each had a 304W coupon suspended horizontally in both the vapor and the liquid phases.

## 2.1 Quality Assurance

Requirements for performing reviews of technical reports and the extent of review are established in manual E7 2.60. The SRNL Technical Report Design Checklist contained in WSRC-IM-2002-00011, Rev. 2 was used as guidance for the technical review of this document.

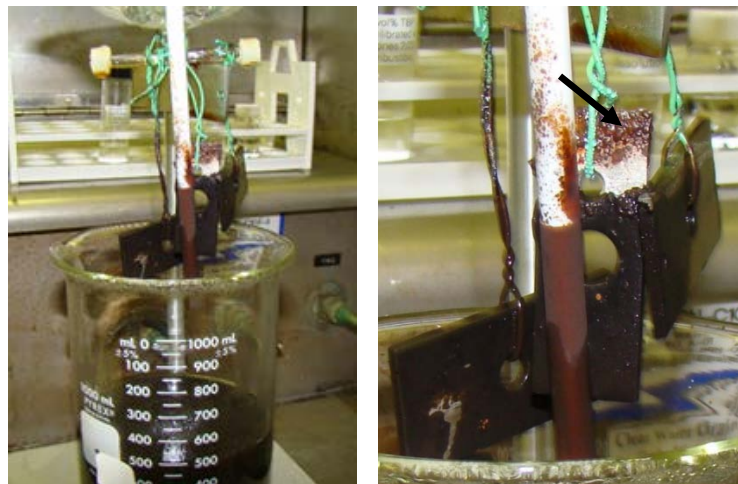
### 3.0 Results and Discussion

Preliminary test observations will be presented and discussed followed by the post-test corrosion assessment of the test coupons.

#### 3.1 Observations on Test 1 Reillex HPQ Batch 1364.1 chloride form resin

This test was intended to reproduce the conditions of the initial Woodham<sup>8</sup> HGR test. Past work<sup>5</sup> noted the extensive quantity of MnO<sub>2</sub> produced by resin digestion but the deposition of a MnO<sub>2</sub> coating on the metal and Teflon™ surfaces had not been previously reported. In most cases, past work was performed in glass laboratory vessels. While there was no independent confirmation that this coating was MnO<sub>2</sub>, past experience<sup>5,2</sup> and the chemistry of the reaction of permanganate with organics<sup>6</sup> gives a strong reason to believe that this coating is MnO<sub>2</sub>. Woodham<sup>8</sup> used a stainless vessel and did not report the formation of a coating; however, a visual examination of the vessel used in that previous test had obvious residual MnO<sub>2</sub>. The glass beaker did not have MnO<sub>2</sub> coating at the liquid interface for Test 1 although some of the later tests did have a coating at the interface. At the start of all the tests, the solution was a deep purple color from the permanganate.

The non-welded coupon (304L #10) has a corroded area near the hanger wire in the upper portion of the coupon. In Figure 3-1, this area is covered with reddish rust as indicated with the black arrow. In Figure 3-2, this area is discolored. The coupon weight loss was not consistent with the



a) Coupons above the solution      b) Close-up of coupons

Figure 3-1. Coupon appearance at the end of a 15-h acidic digestion - Test 1 chloride form resin.



Figure 3-2. Coupons from Test 1 after cleanup. (from left to right) vapor, interface, submerged welded coupons, and non-welded coupon at the interface. Black arrow denotes area with accelerated corrosion near position of uncoated hanger wire.

other coupons and it was postulated that condensation of acidic fumes may have corroded the end of the copper-based hanger wires used to suspend the coupons. In subsequent tests, the ends of these wires were coated with epoxy to avoid this potential problem. Generally, these coupons had some visible corrosion and suspect pitting as determined macroscopically like that observed in the HGR testing.

A sample of this resin was analyzed by neutron activation analysis (NAA) for chloride at 57,800  $\mu\text{g Cl/g}$  wet resin (semi-quantitatively, i.e., outside the range of the calibration standards). The sample was submitted damp (after filtering and air drying but not vacuum drying). Moisture content biases the analysis for chloride to be low because it increases the sample mass. Stiemke<sup>10</sup> determined that the conversion from wet resin to oven-dried resin was a factor of three for Reillex HPQ resin but this value is likely sensitive to the technique. Using the Steimke conversion factor of three, this resin sample could have been as high as  $\sim 170,000 \mu\text{g Cl/g}$  dry resin, however that may be too conservative of an estimate for the water content. This high value for chloride is consistent with the value expected for a chloride form resin. Based on these chloride values, the solution in the test was 600-900  $\mu\text{g Cl/mL}$  solution, which was sufficient to cause localized corrosion for 304L. Woodham<sup>8</sup> measured chloride values after adjustment to 1M hydroxide of 185 and 142  $\mu\text{g/mL}$ . While these chloride values do not compare that well, the uncertainties in both analyses are high and not readily quantified. The main conclusion to draw is that the resin sample was primarily a chloride form resin and orders of magnitude higher in chloride than the HB-Line resin specification.

### 3.2 Observations on Test 2 Reillex HPQ HB-Line nitrate form resin sample

The Test 2 digestion progressed similarly to that of Test 1. It was observed that the solution lost to evaporation was  $\sim 20 \text{ mL}$  (or 0.13 inch of level). A similar rate of evaporation was assumed to have occurred for Test 1, but that aspect of the test was not as closely observed. During the initial stages of the test, splashing of small droplets of permanganate solution occurred throughout the interior of the vessel (Figure 3-3a). Further observations during Test 2a suggest that this splashing is due to bubbles of gas bursting at the surface of the solution. At the end of the test (15 h), the purple color was gone from the solution and most of the purple droplets were washed back down into the bulk solution by condensation (Figure 3-3b). Figure 3-4 shows the location of the liquid interface on the coupons. Note that there is evidence of a  $\sim 0.75$  inch “bathtub-ring” coating the inside of the beaker as seen in Figure 3-4 and Figure 3-5a. The true liquid level in Figure 3-4 is at the 450-mL mark rather than the 500-mL mark (see marking on rear of beaker).

Figure 3-5b shows the  $\text{MnO}_2$  coating that remained on a coupon after the initial water rinse. Further cleaning by immersion into a nitrous acid solution removed all the bulk  $\text{MnO}_2$  but a small amount of stain remained (Figure 3-5c). After cleaning, there was visual evidence of corrosion on the submerged welded areas of the coupons but not in the vapor phase (Figure 3-6). There was some residual stain from the  $\text{MnO}_2$  but there was no evidence of suspect pitting as observed in Test 1.

---

<sup>10</sup> J. L. Stiemke, M. R. Williams, T. J. Steeper, R. Leishear, “Nitrate Conversion of HB-Line Reillex™ HPQ Resin”, SRNL-STI-2012-00160, Rev. 0, Savannah River National Laboratory, May 2012.

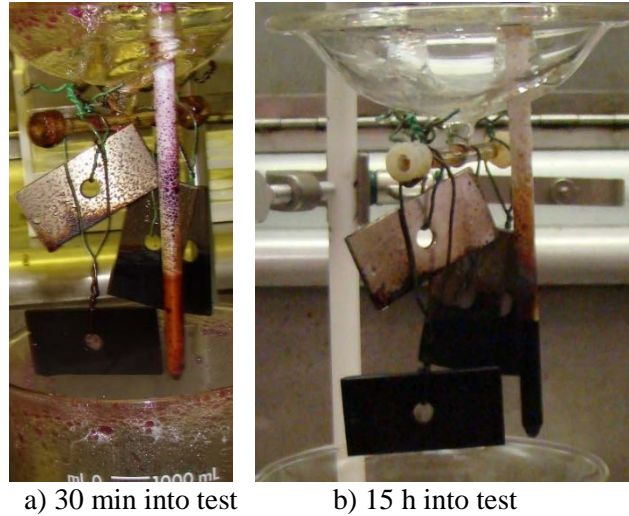


Figure 3-3. Coupon appearance raised above beaker in Test 2 nitrate form resin. Note purple color from permanganate is absent in 15-h photo.

A sample of this resin was analyzed by neutron activation analysis (NAA) for chloride at  $79.5 \mu\text{g Cl/g}$  wet resin (29.2% 1 sigma uncertainty). On a dry resin basis (using the 3x Stiemke conversion), this sample was  $\sim 240 \mu\text{g Cl/g}$  dry resin which is consistent with the value expected for a nitrate form resin. Based on these values the solution was  $\sim 1.0 \mu\text{g Cl/mL}$  solution.

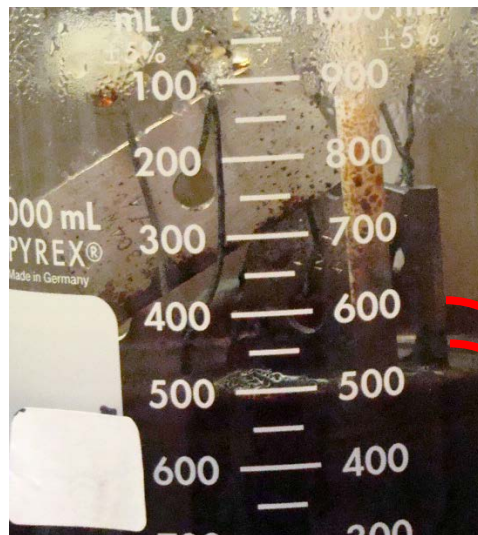


Figure 3-4. Coupon location relative to solution level 14.5 h into Test 2.

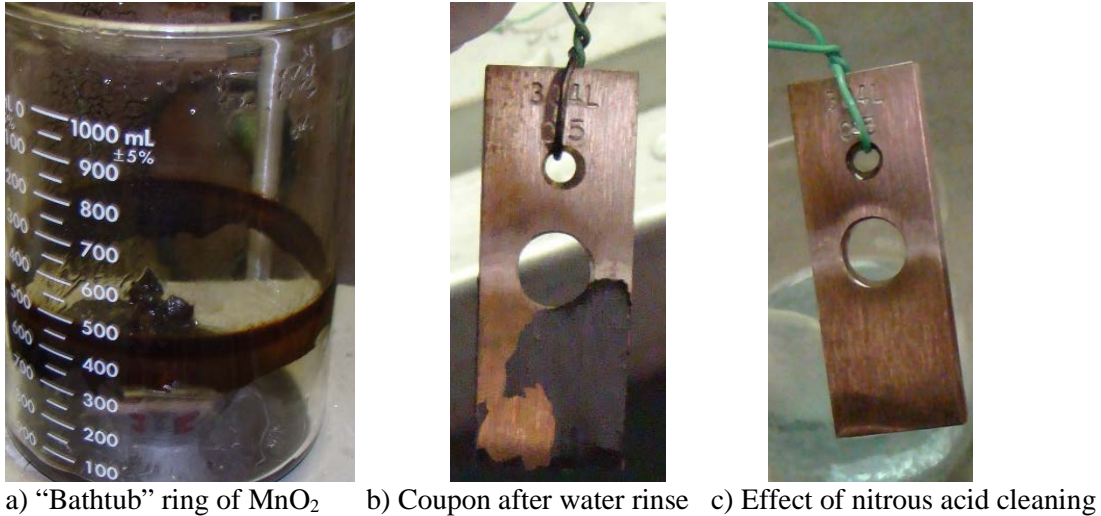


Figure 3-5. Test 2 cleanup showing MnO<sub>2</sub> coating on beaker and coupon #05.

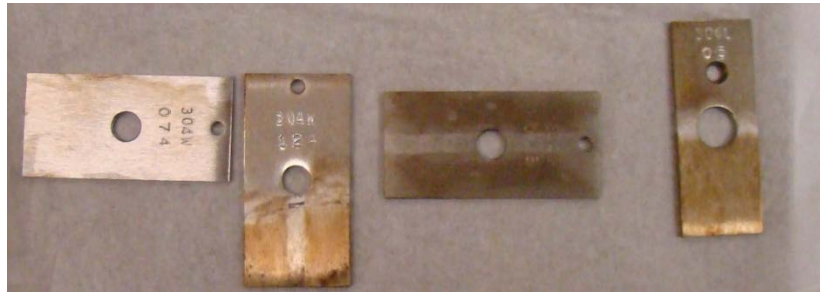
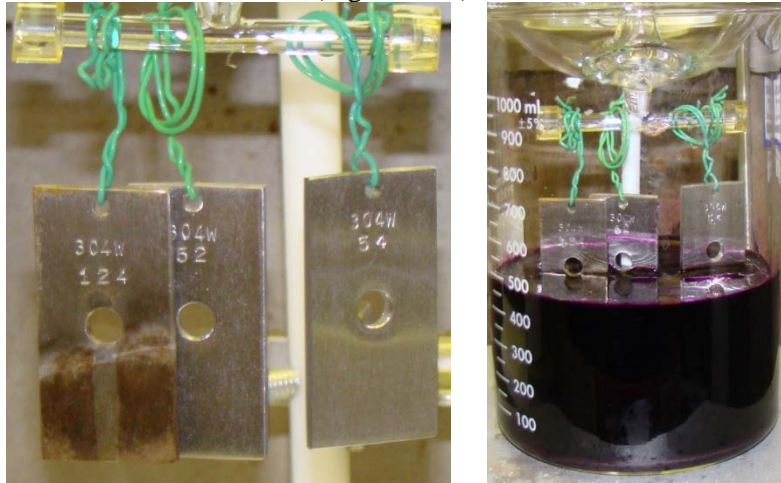


Figure 3-6. Coupons from Test 2 after cleanup: (from left to right) welded vapor, welded interface, welded immersed, and non-welded interface. Staining is prevalent on the coupons.

### 3.3 Observations on Test 2a Reillex HPQ HB-Line resin sample (Nitrate form resin)

This test used the same chemical conditions as Test 2 but was performed during the day-shift so that the test could be monitored periodically (~ hourly) and was performed for only 5 hours, whereas Test 2 was performed for 15 hours. The persistence of permanganate and the development of the MnO<sub>2</sub> layer was monitored. Additionally, this test provided the opportunity to re-expose a coupon to the acid digestion to simulate the two acid digestions conducted in Tank 5.2. Coupon #124 from Test 2, which was exposed in a vertical interfacial position, was re-exposed in Test 2a in the same type position. Figure 3-7 through Figure 3-12 show the progression of the MnO<sub>2</sub> layer and the coupon surfaces over the course of the test. Figure 3-7 shows the appearance of the coupons at the beginning of the test and the solution level on the coupons. Figure 3-8 shows the splatter of permanganate on the coupons and the thermocouple and wire supports just 30 minutes into the test. After three hours into the test (Figure 3-9) the purple color of permanganate was not prevalent on the coupons, but the solution was still purple. The rate of gas bubble formation was significantly reduced from the initial hour of the test. Four hours into the test (no picture shown), a drawn sample of the solution was noticeably paler in color but still purple. After five hours of heating, the solution color was obviously different. Figure 3-10 shows the coupons at that time. Even though there is a drop of purple-colored solution hanging from a wire, the coupons and supporting hardware have been washed down with condensed liquid leaving minimal permanganate on the upper surfaces of the test vessel. Figure 3-11 shows that the pH adjustment with caustic had a slight effect on the

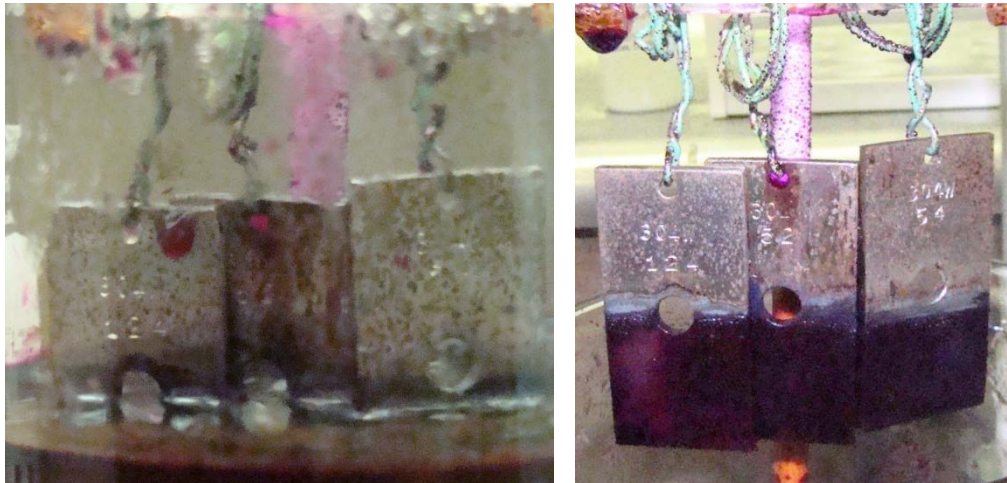
MnO<sub>2</sub> coating but most of the coating remained intact until the coupons were cleaned with water washing and then nitrous acid treatment (Figure 3-12).



a) Coupons hanging prior to test

b) Coupons and solution level

Figure 3-7. Start of Test 2a



a) Coupons in solution

b) Coupons suspended above solution

Figure 3-8. Appearance of coupons: 30 min into Test 2a.



a) Coupons in solution

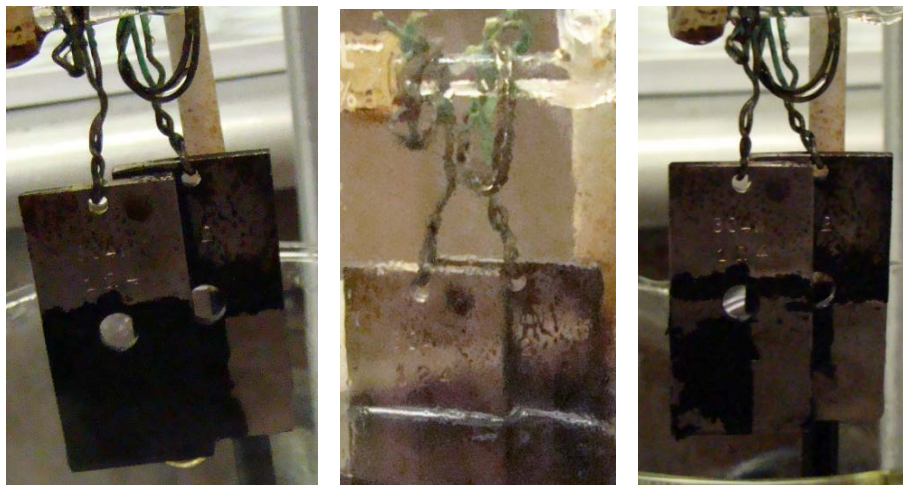
b) Coupons suspended above solution

Figure 3-9. Appearance of coupons: 3 h into Test 2a.



a) Coupons in solution      b) Coupons suspended above solution

Figure 3-10. Appearance of coupons: 5 h into Test 2a.



a) Before caustic addition    b) Submerged      c) After caustic addition

Figure 3-11. Coupons before and after caustic adjustment.



Figure 3-12. Corrosion coupons from Test 2a after cleaning. (304W #124 exposed to both Test 2 and 2a, 304W #124 and #52 exposed through neutralization step, 304W #54 removed prior to neutralization step)

### 3.4 Observations on Test 3 Reillex HPQ HB-Line resin sample (nitrate form resin) Neutral pH

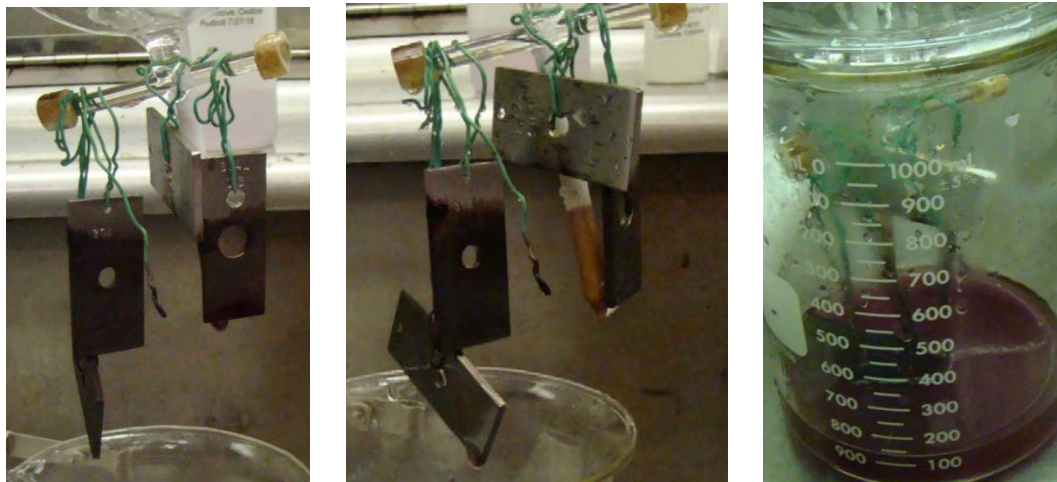
Test 3 was included to assess the effect of the traditional resin digestion flowsheet on stainless steel. It has been assumed that pH of the traditional flowsheet varied significantly<sup>5</sup> from the pH 8-10 called for in the Synder<sup>1</sup> document. In the current test, the pH was adjusted to the range of 4-8 (using pH paper) prior to the addition of the permanganate. The digestion proceeded similarly to Tests 1 and 2. Gas bubbles were more noticeable early in the test but as time progressed the number of bubbles declined. Figure 3-13 shows the solution interface level on the coupons. At the completion of the 15-hour digestion cycle, the coupons were removed and hung above a clean beaker. Unlike the other tests, the bulk solution was still purple indicating excess permanganate was present after the digestion was complete. The final digestion solution was filtered and there was little or no evidence of resin solids present. Although the coupons were stained, the MnO<sub>2</sub> coating was not present as it was in the other tests.



a) Start of test

b) End of test

Figure 3-13. Position of coupons in solution Test 3.



a) Coupons prior to water rinse

b) Coupons after water rinse

c) Rinse solution (purple)

Figure 3-14. Coupon cleanup.

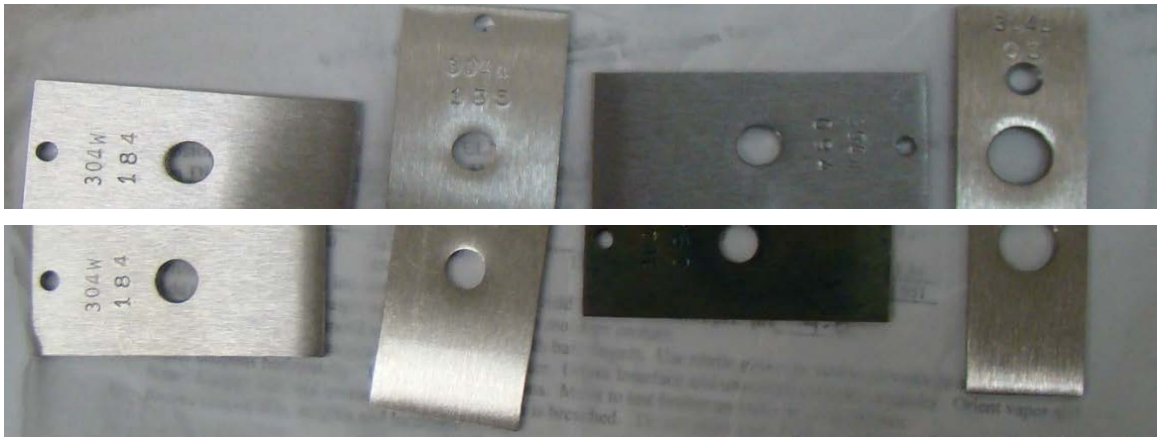
The reduced generation rate of gas bubbles and the persistence of permanganate may indicate that the reaction rate is lower under these conditions. Figure 3-14 shows the coupons before and after cleaning with a water rinse. Without the relatively thick coating, these coupons cleaned easily with

the nitrous acid wash. Figure 3-15 shows coupon 304L #05 during cleaning. A 2-second “dip” in the nitrous acid solution cleaned the coupon to a “like-new” appearance.

The submerged coupon from this test was not nitrous acid cleaned. The weight loss (see Table 3-1) was essentially zero for this test for all coupons. Figure 3-16 shows the appearance of all four coupons before and after the test.



a) Water rinsed    b) Dipped in nitrous acid for 2 s    c) Immersed for 2 s  
Figure 3-15. Nitrous acid cleaning- Coupon 304L #05.



a) Above-pre-test    b) Below post-test-submerged coupon not cleaned  
Figure 3-16. Test 3 Pre- and post-test appearance of coupons.

### 3.5 Corrosion Assessment of Test Coupons

The corrosion of stainless steel exposed to nitric acid-based solutions consists of both general corrosion and any localized corrosion, which depends on the specific conditions of the environment. In the case of the resin acid digestion, the oxidizing species used for resin destruction, potassium permanganate, creates a highly oxidizing condition for the stainless steel, which is the material of construction of Tank 5.2. Oxidizing conditions are known to facilitate intergranular attack (IGA), including weld interdendritic attack, for stainless steel.<sup>11</sup> Although chloride is not a common solution constituent for canyon processes, its presence in the Woodham HGR test may have accelerated IGA and led to suspect pitting, especially at the air/liquid interface<sup>8</sup> (see Appendix for

<sup>11</sup> A. J. Sedriks, Corrosion of Stainless Steel, 1997, J. Wiley & Sons,

the preliminary corrosion assessment that was performed on the Woodham test equipment). Although chloride was present in the Woodham test resin, the Reillex resin used in H-Canyon contains less than 250 ppm total chloride.<sup>10</sup> These test results demonstrate the significant corrosion of stainless steel from the acid digestion process and indicate the possible impact chloride can have on the corrosion process.

The general corrosion rate calculation will be discussed first followed by the localized corrosion observations. The localized corrosion results for Tests 1, 2 and 3 will be presented and discussed together by exposure condition: vapor-exposed coupons, interfacial coupons and fully immersed coupons. Test 2a results will be discussed separately since the emphasis was on the cumulative impact of successive acid resin digestion batches.

### 3.5.1 General Corrosion Rate

The general corrosion rate provides a broad measure of an environment aggressiveness to a material. In the case of this testing, the general corrosion rate was used to assess a relative impact on stainless steel corrosion of different exposure conditions. The exposures correspond to the various conditions of process tank wall and cooling coils, including vapor, interfacial, and fully immersed. The average corrosion rate for each coupon was calculated based on the weight loss as well as the exposed surface area and time of exposure as given in Equation 1<sup>12</sup>

$$CR = (K * W) / (\text{surface area} * \text{time} * \rho) \quad (1)$$

where K is a constant ( $3.45 \times 10^6$  for units of mils per year (mpy)), W is mass loss (grams (g)), surface area is for the coupon ( $\text{cm}^2$ ), time is exposure time (hours), and  $\rho$  is the material density ( $\text{g}/\text{cm}^3$ ). The primary assumption for this equation is that corrosion is uniform across the exposed surface. Table 3-1 contains the weight loss and corrosion data for all four tests. The negative corrosion rate measured in Test 3 for one of the coupons may be measurement error or an indication of oxide growth.

A review of the table shows that the overall trend of a decreasing general corrosion rate is in the order of liquid, interfacial and vapor exposures. This trend is slightly misleading since a true interfacial only coupon was not tested, although attempts were made during Test 1. The interfacial coupons had large areas that were exposed only to the vapor or liquid. Areas close to the air/liquid interface varied in their exposure since the interface lowered during the experiment due to evaporation. The measured interfacial corrosion rates fall between the vapor and liquid only corrosion rates and depend on the actual areas exposed in the vapor and liquid. For Test 1, where the 304W interface coupon had greater area immersed, the corrosion rate is closer to the fully immersed rate (78 versus 91 mpy, respectively), while for Test 2 where the 304W coupon was more evenly positioned between the vapor and liquid, the interfacial corrosion rate (47 mpy) falls nearly in the middle of the vapor and liquid only corrosion rates (4 and 94 mpy, respectively).

The test results for Test 2a show several factors about the corrosion during acid digestion. First, a comparison of the corrosion rate of Coupons #52 and #54 from Test 2a to that for Coupon #124 from Test 2 show corrosion rates (83 and 91 mpy from Test 2a versus 44 mpy for Test 2) are double for test times that are approximately half as long (8 hours for Test 2a and 15 hours for Test 2). These differences indicate that the most corrosion occurs early during the process, which is probably associated with the permanganate activity. As stated earlier, a Test 2a observation was that permanganate activity appeared to be reduced after 4-5 hours of testing.

<sup>12</sup> ASTM G1 "Standard Practice for Preparing, Cleaning, and Evaluating Corrosion Test Specimens."

The second factor learned from the Test 2a results was that a corroded surface has a higher corrosion rate when re-exposed. The corrosion rate for Coupon #124 during Test 2a was 133 mpy, which was much higher than the rates of the other Test 2a coupons (#52 and #54 with rates of 83 and 91 mpy, respectively). Coupons #52 and #54 were new coupons unexposed prior to Test 2a, while Coupon #124 had suffered IGA during the Test 2 exposure.

The presence of chloride impacts localized corrosion, such as pitting, but except at very high levels would not be expected to impact the general corrosion rate, which was the result observed in this testing. A comparison of the Tests 1 and 2 results show that for the 304W coupons the vapor and liquid exposure corrosion rates did not show any difference. The 304L coupon data cannot be compared because of the accelerated corrosion noted earlier that occurred on the 304L coupon from Test 1.

Table 3-1. Corrosion Coupon Weight Loss

		Weight				Corrosion Rate
Test 1		Coupon	Pre-Test	Post-Test	Loss	
Reillex HPQ Batch 1364.1		ID	g	g	g	mpy
Vapor	304W	160	26.289	26.287	0.002	2
Horizontal	304W	091	26.869	26.789	0.079	78
Liquid	304W	140	26.857	26.764	0.093	91
Vertical	304L	10	20.171	19.955	0.215	274
Test 2						
Reillex HPQ HBL Sample						
Vapor	304W	074	26.121	26.117	0.004	4
Vertical	304W	124	27.098	27.050	0.048	47
Liquid	304W	148	26.660	26.564	0.096	94
Vertical	304L	05	20.463	20.428	0.035	45
Test 2a						
Reillex HPQ HBL Sample						
Vertical	304W Used	124	27.050	26.977	0.073	133
Vertical	304W	54	27.787	27.742	0.046	83
Vertical	304W	52	27.785	27.735	0.050	91
Test 3						
Reillex HPQ HBL sample pH 4-8						
Vapor	304W	184	26.925	26.925	0.000	0
Vertical	304W	135	25.660	25.660	0.000	0
Liquid	304W	094	26.455	26.456	-0.001	not cleaned
Vertical	304L	05	20.684	20.684	0.000	1

\*The coupons with an air/liquid interface were oriented either vertical or horizontal

The general corrosion rates for the vapor-exposed coupons, 0-4 mpy, are very low.<sup>13</sup> The rates for the remaining coupons are significant and may be considered acceptable depending on various

<sup>13</sup> P. A. Schwietzer, Corrosion Resistance Tables, 3<sup>rd</sup> Ed, Marcel Dekker Inc, New York NY, 1991

factors such as wall thickness, intended service life, and use duration. The liquid-exposed corrosion rates at ~90 mpy are not advantageous for prolonged use of components. The problem for this type digestion, however, is not general corrosion, but rather localized corrosion. The key is the depth of penetration which is discussed for each test in the following section.

### 3.5.2 Localized Corrosion Observations – Tests 1, 2, and 3

In these three tests, 304W coupons were exposed in the vapor space only, in liquid only, and with an air/liquid interface. The environment conditions for these three exposure conditions impacted the occurrence of localized corrosion. A non-welded 304L coupon was also exposed with an air/liquid interface.

#### 3.5.2.1 Vapor Exposure

In all three tests, the vapor exposure conditions were the least corrosive with minimal localized corrosion occurring on the stainless steel coupons, which coincided with low general corrosion rates. The acid digestion coupons showed some rust staining and oxide discoloration, while the neutral pH digestion coupons appeared almost like new with limited oxide discoloration. Figure 3-17 shows the vapor-exposed 304W coupons from Tests 1 (chloride form resin with acid digestion) and 3 (nitrate form resin with neutral pH digestion). The rust staining on the coupon from Test 1 can be seen on the left-hand side of the photograph.



Figure 3-17. Vapor-exposed coupons from Tests 1 (#160, acid digestion) and 3 (#184, neutral pH digestion) using nitrate form resin

#### 3.5.2.2 Liquid Exposure

The visual appearance of the 304W coupons from Test 1 (chloride form resin, acid digestion) and Test 2 (nitrate form resin, acid digestion) were similar with an irregular surface stain on the base metal (see Figure 3-18). The Test 3 (nitrate form resin, neutral pH digestion) interfacial coupon had minimal residual staining on the lower half of the coupon which was exposed to the solution. The back side of the coupons are shown where both stained and unstained areas are readily discernible for coupons from Tests 1 and 2. The cause of these unstained areas is not known but may be associated with non-uniform adherence of the  $MnO_2$  layer that deposited across the entire surface as discussed earlier and with handling during the welding process since similar marks were observed on other welded coupons.

The acid digestion coupons had IGA as the predominant corrosion mode along with grain dropout as shown in Figure 3-19. Large areas of grain drop out are shown by the highly irregular surface profile and non-defined edge as shown in Figure 3-20 for the liquid exposed coupon from Test 2.

Pitting corrosion was not definitely identified as prototypical hemispherical pits on these coupons. The observed degradation was associated with some degree of grain boundary interaction. Pitting cannot be discounted since 100% inspection of the surfaces was not performed. Additional testing, such as cyclic polarization testing, would be required for a more definitive evaluation of pitting.

The presence of chloride ions could further accelerate the observed depth of attack, but with the measurements made this was not observed. The depth of penetration in Figure 3-20 measured  $27\ \mu\text{m}$  (1.1 mils). On the coupon from the chloride form resin digestion (Test 1) depths generally measured between 10 and  $15\ \mu\text{m}$  (~0.5 mils). In welds, maximum measured depths were higher ( $36\ \mu\text{m}$  (1.4 mils)). The more significant corrosion in the weld was measured as the greater width of this pit. The weld corrosion occurs by preferential corrosion of the interdendritic areas first, similar to IGA for the base metal (see Figure 3-24 for an example of interdendritic attack).

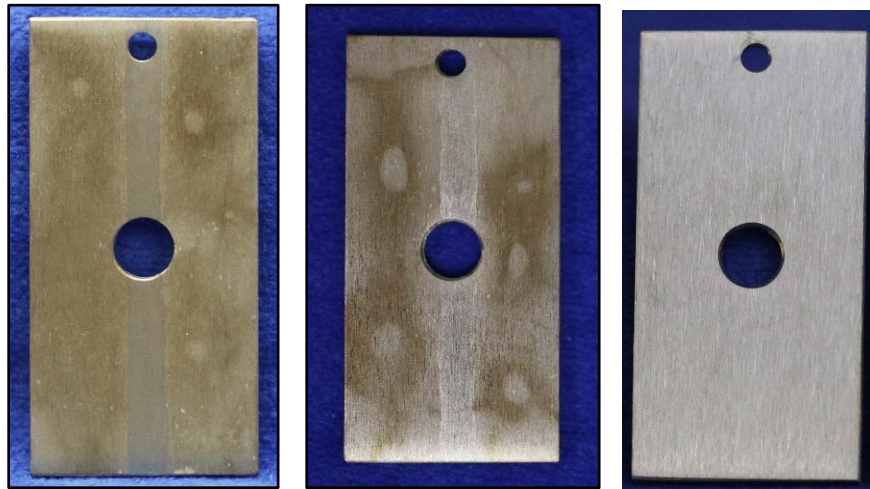


Figure 3-18 Liquid-exposed coupons from Test 1 (left, acid digestion) and Test 2 (middle, acid digestion) and the vertical interfacial coupon from Test 3 (right, neutral pH digestion).

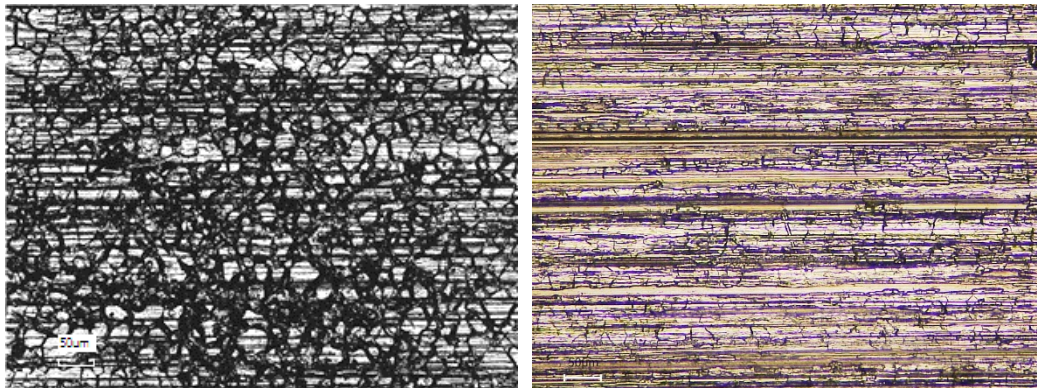


Figure 3-19 Micrographs (200x) showing the intergranular attack observed on the immersed coupon from Test 1 using the chloride form resin acid digestion

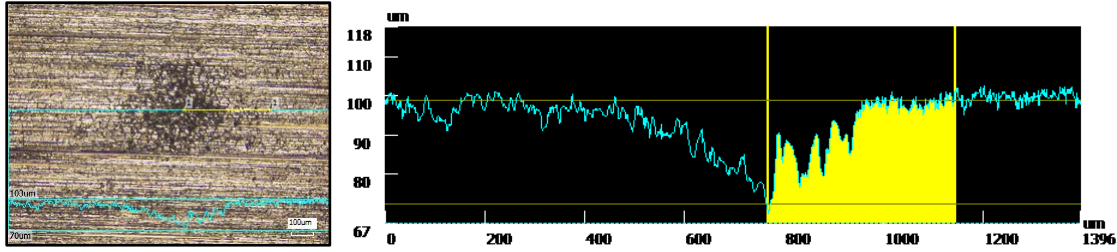


Figure 3-20. Micrograph (100x) of immersed 304W coupon (#148) after a 15-hour acid digestion of the nitrate form resin at 76 °C (Test 2) showing IGA on the surface along with an area of grain drop out; line profile through area of grain drop out



Figure 3-21. Test coupons from Test 3 after 15 hours of the nitrate form resin neutral pH digestion performed at 76 °C; coupons are shown in the following order: 304W vapor-exposed only, 304W interfacial exposure, 304W liquid-exposed only (not cleaned in nitrous acid), 304L interfacial exposure.

As shown in Figure 3-21 the neutral digestion coupon (304W #094) from Test 3 was different in appearance with a residual blue stain at the surface since it was not cleaned in nitrous acid like the other coupons as discussed earlier. However, the interfacial coupons (304W #135 and 304L #03) with approximately half the surface immersed in the liquid, which were cleaned in the nitrous acid as all the other test coupons, were not colored. The surfaces on these coupons showed no signs of intergranular attack or accelerated attack of the weld to highlight its presence.

### 3.5.2.3 304W Air/Liquid Interface

The original plan for these coupons was to have the interface across the length of the coupon with equal portions in the vapor and the liquid, but in Test 1, the interfacial 304W coupon slipped so most of the coupon was immersed with a minimal vapor-exposed portion of the coupon. For Tests 2 and 3, the interfacial 304W coupons were oriented vertically like the 304L coupons. The numbered side of the interfacial 304W coupons from Tests 1-3 are shown in Figure 3-22 for comparison (a dotted line shows the approximate location of the interface). The interface can be seen for both Test 1 (angled by the lower left corner of coupon) and Test 2 (slightly angled across width below central coupon hole). The air/liquid interface cannot be seen on the Test 3 coupon, an indication of the minimal corrosion that occurred. The lack of visual corrosion agrees with the negligible weight gain, which could occur with oxide growth or possible measurement error.

For Test 1, the coupon had similar corrosion morphologies on the vapor-exposed and liquid-exposed portions of the coupons as those discussed previously. The vapor-exposed portion showed some staining and slight IGA since most of the vapor-exposed area was close to the liquid. The liquid-exposed portion had IGA, grain drop out and pitting similar to that discussed above for the liquid exposed coupons. The pit-like features had similar depth measurements 10-15  $\mu\text{m}$  (0.4-0.6 mil). At the interface, however, the corrosion was more extensive as noted by wider areas of IGA and trenching (a coalescence of individual areas of grain dropping or pitting) with a depth of 35-40  $\mu\text{m}$  (1.4-1.6 mils) resulting from localized attack near the interfaces. Figure 3-23 shows this attack in a LCM micrograph and corresponding height scan for an interfacial area on the Test 1 304W coupon. Point measurements in the weld found a depth at 44  $\mu\text{m}$  (1.7 mils).

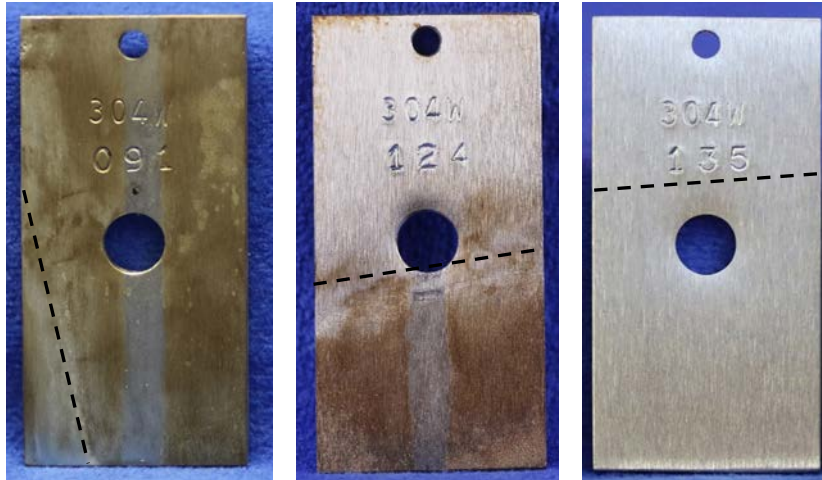


Figure 3-22 Interfacial 304W coupons after resin digestion tests with: (left) Test 1- acid digestion, chloride form resin; (middle) Test 2 - acid digestion, nitrate form resin; and (right) Test 3 - neutral pH digestion, nitrate form resin

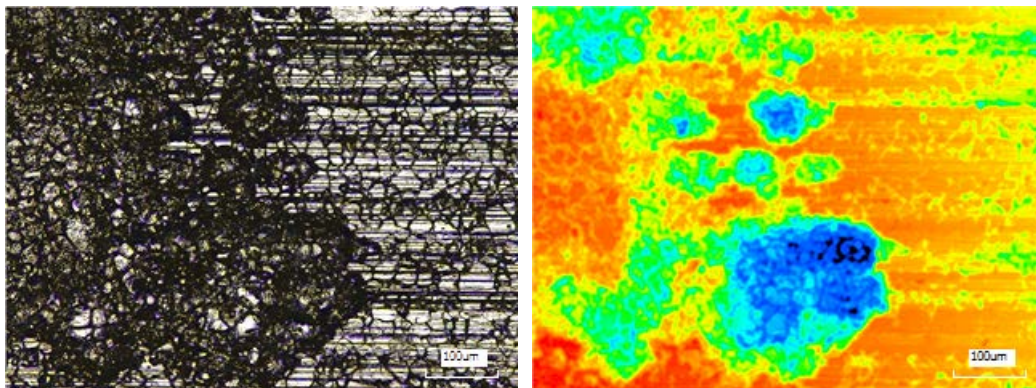


Figure 3-23. Interfacial region from 304W coupon after 15-hour acid digestion at 76 °C of chloride form resin (Test 1)

For the Test 2 coupon, the overall degradation was similar to that observed on the vapor only and liquid only exposed coupons. The vapor portion of the interfacial 304W coupon had greater staining and some slight IGA, while the liquid portion had IGA prominent along with areas of grain drop out. The depths of these areas were approximately 20  $\mu\text{m}$  or 0.8 mils. At the air/liquid interface as shown in Figure 3-24, the corrosion was more extensive with wider areas of IGA; the measured trenching was 12-18  $\mu\text{m}$  (0.5-0.7 mil). The corrosion in the weld as noted by a depth of

~36  $\mu\text{m}$  (1.4 mil) was greater than the surrounding base metal. These measurements were comparable to those measured on the coupon from Test 1 during the chloride form resin digestion.

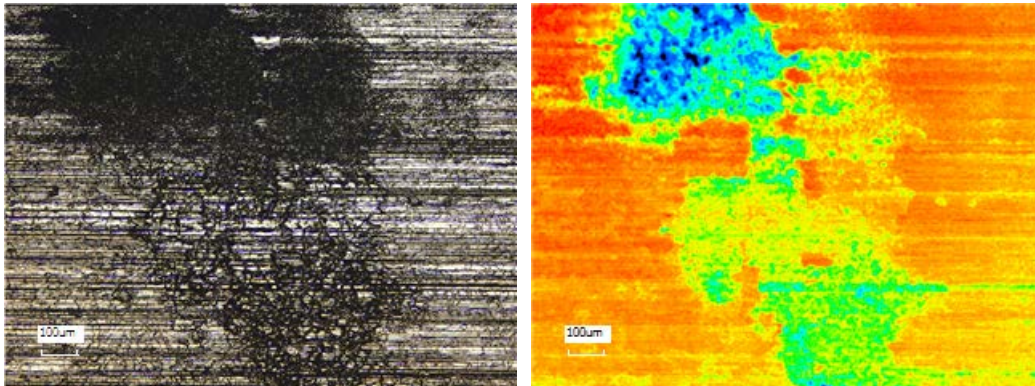
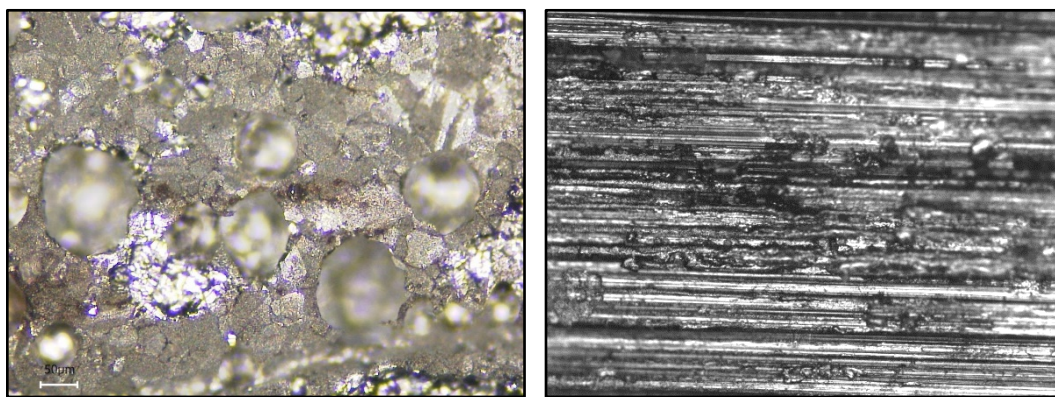


Figure 3-24. Interfacial region near the weld from 304W coupon after 15-hour acid digestion at 76 °C of nitrate form resin; weld is the upper half of micrograph and height scan (Test 2)

#### 3.5.2.4 304L Air/Liquid Interface

The interfacial 304L coupons had similar corrosion to the other coupons in each test except for Test 1. As previously discussed, the Test 1 (chloride form resin) coupon had a preponderance of pitting and surface etching in the vapor portion that resulted from the wire condensate dripping on to the coupon. The presence of the copper ions in the condensate may have added to the aggressiveness of the condensate, which otherwise would be nitric/nitrous acid. The impact of the copper ions in the solution was not expected to be significant because of dilution. The corrosion observed on the remainder of the coupon was far less severe with no significant IGA and random pitting on the liquid portion. The corrosion morphologies of the vapor and liquid portions of the interfacial 304L coupon are shown in Figure 3-25.



a) Vapor phase

b) Liquid phase

Figure 3-25. The corrosion morphology of the vapor and liquid portions of the Test 1 304L coupon

The Test 2 304L coupon had similar corrosion characteristics to the 304W coupons from that test. In the vapor-exposed portion of the coupon, slight grain boundary highlighting was observed along with rust-colored corrosion products. The liquid portions of the coupon clearly demonstrated areas of IGA along with localized spots of grain drop out (~ 25  $\mu\text{m}$  (1 mil) depth). There appeared to be more areas of grain drop out on the 304L coupon than the 304W coupon. The interfacial portion

of the coupon had significant widening of the IGA as compared to the immersed portion of the coupon. Widths of 25  $\mu\text{m}$  (1 mil) were measured while on the immersed portions widths were not measurable at the examination magnification (100-200x). The degree of IGA decreased in either direction towards the vapor or immersed portion of the coupon as shown by the micrographs in Figure 3-26.

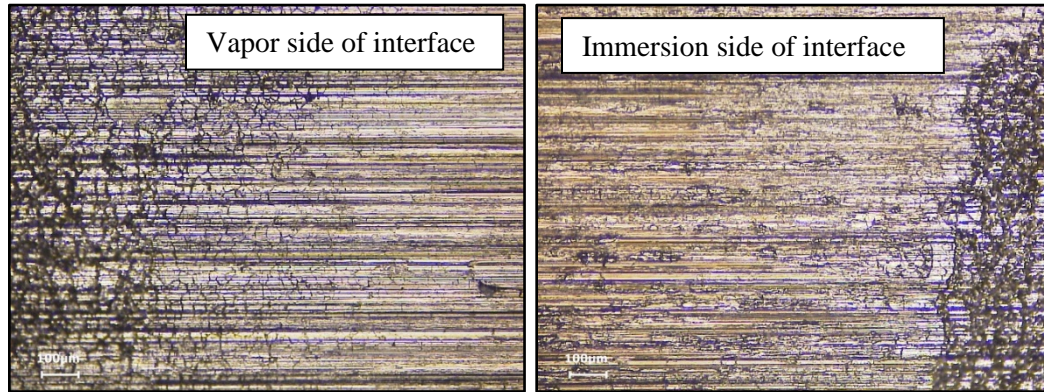


Figure 3-26.. Micrographs (100x) of the air/liquid interface 304L coupon (#05) from nitrate form resin acid digestion test after 15 hours at 76 °C (Test 2)

The Test 3 coupon, as shown previously in Figure 3-21 (304L #03), showed only some slight oxide discoloration. None of the Test 3 coupons showed any notable corrosion.

The interfacial area on both the 304W and 304L coupons from Tests 1 and 2 have shown the greatest degradation as indicated by the widest IGA openings at the surface as well as the greatest depths of pitting or grain drop out. Sections of the interfacial areas of the 304L coupons were removed and mounted to examine the corrosion profile to assess further the depth of corrosion and the mechanism(s). Additionally, the surface depth measurements performed using the LCM could miss the full depth of penetration since undercutting of grains would not be detected as the LCM uses line of sight for the reflecting signal.

Figure 3-27 shows the reconfigured 304L coupons from Tests 1 and 2 after sectioning. Areas of vapor, liquid and interfacial exposure were taken from each sample. The mount was ground through a series of finer papers ending with a 1- $\mu\text{m}$  diamond polish. The coupon was examined in both the etched and unetched conditions to demonstrate the association with grain boundaries and to assess the full depth of penetration, respectively. Etching was performed using a standard electrolytic oxalic acid process.

For the Test 1 coupon, the cross-sectional examination revealed that the IGA and pitting appear to be working synergistically as shown in Figure 3-28. In many of the pit-like features shown in these two micrographs, the corrosion appears to be progressing along a grain boundary. IGA may have occurred initially due to oxidizing conditions, but the presence of chloride could assist in transitioning to a pit with the lateral growth of the initial IGA. Additionally, pitting may have initiated at a location within a grain, growing into a boundary thereby setting up conditions for IGA.



Figure 3-27. Sectioned interfacial 304L coupon from Tests 1 (left) and 2 (right); missing section was mounted for cross-sectional examination.

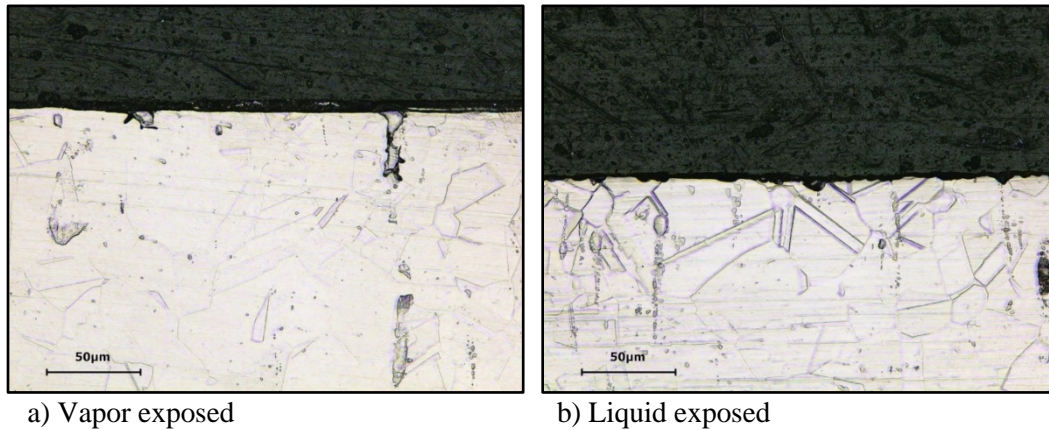


Figure 3-28. Micrographs (500x) showing attack of the air/liquid interface 304L coupon (#10) from chloride form resin acid digestion test after 15 hours at 76 °C (Test 1)

The greatest penetration of depth was observed in the interfacial region which is shown in Figure 3-29 by the montage of several micrographs. The approximate depth of this penetration is 200  $\mu\text{m}$  or 8 mils so the combined effect of IGA and chloride along with highly oxidizing conditions of the air/liquid interface contributed to this material loss. Only one cross sectional plane was examined however.

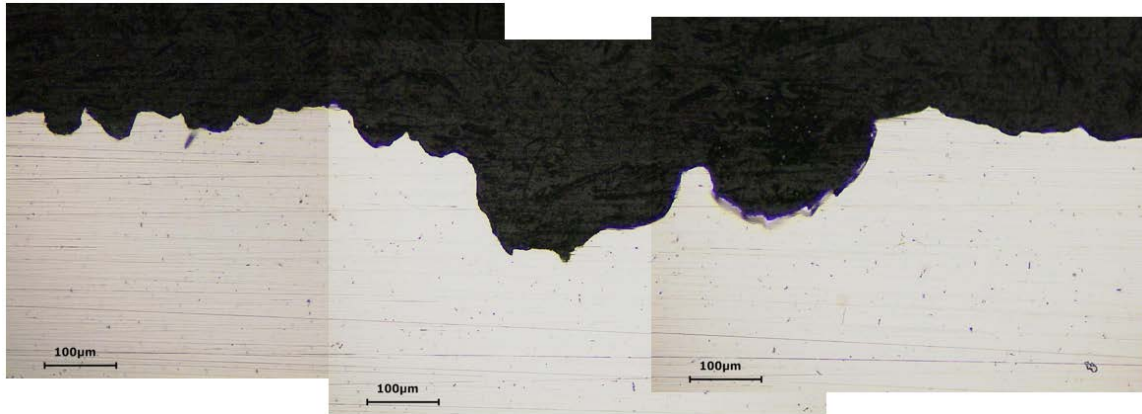


Figure 3-29. Micrograph montage (200x) showing attack in the interfacial region of the air/liquid interface 304L coupon (#10) from chloride form resin acid digestion test after 15 hours at 76 °C (Test 1)

For the Test 2 coupon, the unetched mounted coupon sections showed a maximum depth of penetration of approximately 2 mils although most depths of penetration were on the order of 1 mil, like the LCM measurements. In Figure 3-30, the undercutting and process of grain dropping is clearly observed for the 304L coupon in both the etch and unetched conditions. Only one cross sectional plane was observed so a greater maximum depth of 2 mils may be possible.

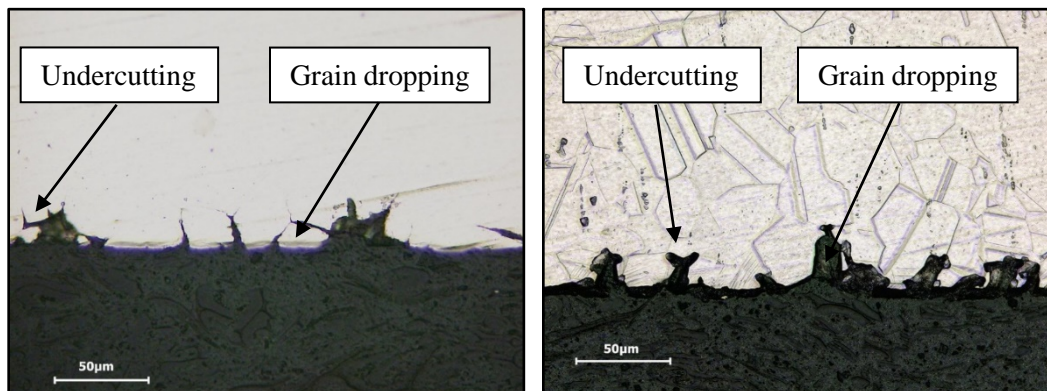


Figure 3-30. Micrographs (500x) of the unetched and etched cross section of an interfacial portion of 304L coupon (#05) from nitrate form resin acid digestion test after 15 hours at 76 °C (Test 2)

### 3.5.3 Test 2a Results

From a corrosion standpoint, Test 2a was performed to re-expose a 304W coupon to acid digestion of the nitrate form resin and assess the effect of multiple exposures on the degradation. Additionally, two 304W coupons were exposed to evaluate whether the final neutralization impacted the corrosion. The overall corrosion that was observed on these coupons was like that observed for Test 2 with IGA and grain drop out being prominent in the liquid with some corrosion staining and slight IGA in vapor portions of the coupons. Figure 3-31 shows these coupons post testing. The two replicate coupons had welds that were across the width of the coupon.

Two coupons, #52 and #54, were examined using the LCM with height scans of typical areas obtained to compare depths and types of attack. As stated above, the observed corrosion was the same as seen in Test 2. Figure 3-31 shows LCM micrographs of typical views for the liquid-exposed area, at the interface, in the vapor-exposed area and for liquid-exposed area of the weld. Depths of attack were similar for these two coupons. Figure 3-31a shows a common spot of accelerated IGA where the depth of attack ranged from 25 - 35  $\mu\text{m}$  (1-1.4 mil) for both coupons, while smaller pit like areas measured  $\sim 20 \mu\text{m}$  (0.8 mil). At the interface, depths of attack (Figure 3-31b) measured 30 - 50  $\mu\text{m}$  (1.2-2 mil) or less while in the welds (Figure 3-31c) depths were closer to 50  $\mu\text{m}$  (2 mil). In the vapor portion (Figure 3-31d), depths of attack were less than 10  $\mu\text{m}$  (0.4 mil).

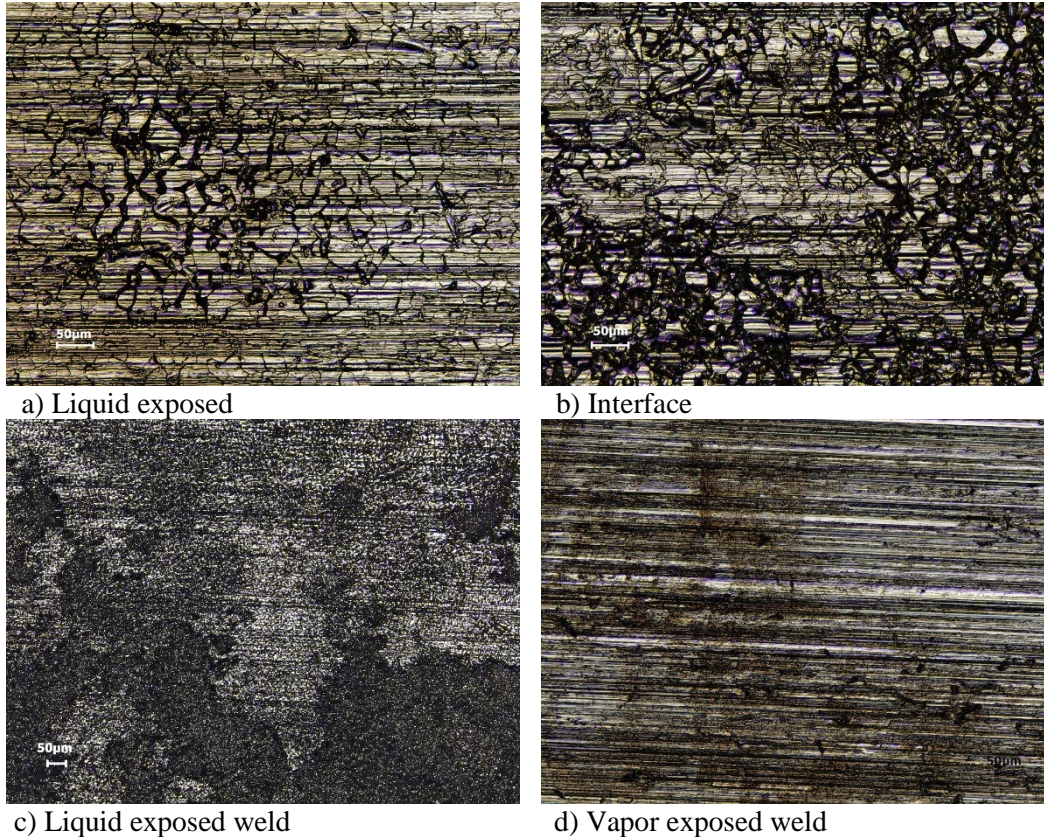


Figure 3-31. Surface corrosion morphology for Coupons #52 and #54 from Test 2a:

The coupon exposed in both Test 2 and Test 2a #124, was found to have similar depths of attack as to those measured for other coupons with weld attack measuring up to 50  $\mu\text{m}$  (2 mil) while areas of grain drop out measured 10-15  $\mu\text{m}$  (0.4-0.6 mil). These measurements were made using the LCM. The interface formed during Test 2a on Coupon #124 did not appear to be coincidental with the interface that formed from Test 2 (see Figure 3-12). So, two sections were removed from Coupon #124 through the interfacial area along the two sides of the coupon to examine the depth of attack from a cross section. The pieces were mounted together and prepared similar to the 304L coupons. Depths up to 60  $\mu\text{m}$  (2.4 mil) were found as shown in the micrograph in Figure 3-32. In this figure, significant undercutting of grains can be seen at numerous locations. Again, only one cross sectional plane was examined.

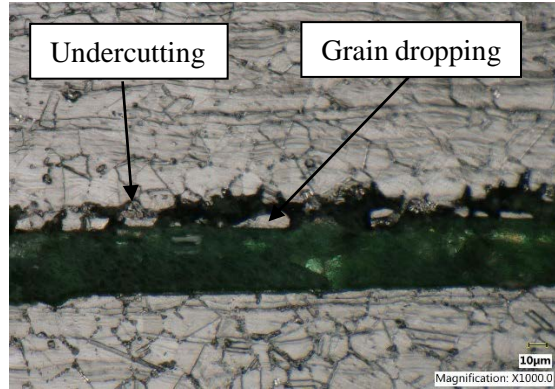


Figure 3-32. Cross section view of interface area for Coupon #124 from Test 2a

The localized corrosion observed in this study demonstrated that IGA was the dominant mode of corrosion for liquid-exposed surfaces and along the air/liquid interface, while on vapor-exposed surfaces staining with only minor grain boundary highlighting was observed. A summary of the test observations for this testing are given in Table 3-2. Possible pitting was observed along the air/liquid interface, but additional testing would be required to be more conclusive.

Table 3-2 Localized Corrosion Observation Summary from Corrosion Testing of Acidic Resin Digestion Process

Test	Resin	Digestion	Exposure	Observed Localized Corrosion	Depth $\mu\text{m}$ , (mil)*
1	Chloride form	Acid	Vapor	Rust staining IGA highlighting IGA	n/a Not measurable
			Liquid	Grain dropout/pitting Weld attack IGA	10-15, (0.4-0.6) 36, (1.4)
			Interface	Grain dropout/pitting Weld attack	35-200, (1.4-8) 44, (1.7)
2	Nitrate form	Acid	Vapor	Rust staining IGA	n/a Width not measurable
			Liquid	Grain dropout Weld attack IGA	20-27, (0.8-1.1) Width 25, (1)
			Interface	Grain dropout/pitting Weld attack	12-50, (0.5-2) 36, (1.4)
2a	Nitrate form	Acid	Vapor	Rust staining IGA	10, (0.4)
			Liquid	Grain dropout Weld attack IGA	20-35, (0.8-1.4)
			Interface	Grain dropout Weld attack	30-60, (1.2-2.4) 50, (2)
3	Nitrate form	Neutral pH	Vapor	None	n/a
			Liquid	None	n/a
			Interface	None	n/a

\*n/a-not applicable

#### 4.0 Implications of Testing

These tests have clearly shown that during acid digestion of resin, either chloride or nitrate form, stainless steel corrodes primarily by IGA, which is similar to the results from the preliminary analysis of the experimental apparatus used in HGR testing (See Appendix). The IGA was prominent for surfaces exposed to the liquid, while for vapor-exposed surfaces generally rust staining occurred. In some cases, grain boundaries were highlighted although with no measurable depth of attack. The HGR test vessel differed in that IGA was present on the vapor-exposed surface. This difference between test results is attributed to difference in the control of the gas in the vapor space. The greatest attack occurred consistently in the interface area with IGA dominant and trench like areas of grain drop out or possibly pitting. Welds consistently had the greatest depth of penetration in these tests as was observed in the HGR test vessel for the circumferential weld which was coincidental with the air/liquid interface. The IGA results from the highly oxidizing conditions of the acid digestion.<sup>14,15</sup>

The presence of chloride from the chloride form resin did not cause obvious greater attack in this testing as can be seen by a visual comparison of the coupons (see Figure 3-22). The presence of more pits or grain drop out or greater depths of attack were not clearly measured on coupons from Test 1 (chloride form resin, acid digestion). While the largest depth of attack was measured in the interfacial cross section from Test 1 with the chloride form resin (Figure 3-29), this measurement was determined from only one cross sectional plane, which was the same for the depth measurement of 2 mils for the coupon from Test 2 (nitrate form resin, acid digestion). This interfacial measurement may indicate more aggressive conditions in the presence of chloride but taking all the results into consideration a more aggressive condition is not supported. Additional measurements on these coupons may provide more convincing evidence. This testing also showed that resin digestion under neutral pH conditions was not corrosive to stainless steel, where there was no measurable corrosion rate or observed degradation of the stainless steel coupons.

The corrosion observed on the coupons from Test 1 with the chloride form resin differed markedly from that observed in the HGR testing experimental apparatus. As noted above, the largest differences were in the corrosion observed on the vapor-exposed surfaces of the test vessel as well as at the air/liquid interface. There were several differences in the way these two tests were conducted which could impact the observed corrosion in each test. First, the HGR test vessel had full penetration welds as opposed to the autogenous welds for the coupons, which would alter the final weld microstructure and fusion zone, possibly leading to greater corrosion. With the circumferential weld coincidental with the air/liquid interface deeper areas of penetration may have occurred that were not observed during Test 1 in the present testing.

The second major difference was the vapor space conditions which is attributed to the different controls for gas handling. In the HGR testing flow rates from the vessel were controlled to low values so that gas analysis could be performed, whereas in the present testing the gas flow was not controlled other than to maximize condensation of moisture. The condensation provided for a wash down of vapor-exposed surfaces as was discussed previously (see Figure 3-3), which removed permanganate containing droplets from the side wall. Whether this wash down occurred in the HGR testing is unclear. If not, residual permanganate on the vapor-exposed surface with the extended duration of the test may have allowed more time for the observed IGA to occur.

---

<sup>14</sup> S. Ningshen, U. Kamachi Mudali, S. Ramya, and Baldev Raj, "Corrosion Behavior of AISI Type 304 Stainless Steel in Nitric Acid Media Containing Oxidizing Species", *Corrosion Science*, 53, 64 (2011).

<sup>15</sup> P. Fauvet, F. Balbaud, R. Robin, Q. T. Tran, A. Mugnier, and D. Espinoux, "Corrosion Mechanisms of Austenitic Stainless Steels in Nitric Media Used in Reprocessing Plants," *Journal of Nuclear Materials*, 375, 52 (2008).

A third difference in the tests operations was the long hold time used during the HGR testing. With the 24-hour room temperature hold, chloride had a longer time to initiate pitting, especially at the interface where resin particulate was floating on the surface. This condition may have caused a local spike in chloride concentration that led to pitting along the interface, further accelerated by the weld microstructure.

In this testing, a layer or coating of  $MnO_2$  formed on the surface of the stainless steel coupons. This layer was thin, brittle and easily removed, in some cases with the water wash. The impact of this layer on the corrosion cannot be clearly stated since this testing was not structured to separate out that effect. Under neutral pH conditions the layer does not form and stainless steel corrosion did not occur. The observed corrosion however is not tied to the layer, since these conditions are known to cause IGA in stainless steel. Since the IGA occurred, the layer may have no impact. Further testing would be required.

Tank 5.2 has been the process vessel for resin digestion for numerous years in H-Canyon using a caustic digestion flowsheet. The last two digestions, however, employed an acid digestion flowsheet with two additional acid digestions proposed. To evaluate the impact of the proposed digestions on Tank 5.2, an assessment of the current material condition for Tank 5.2 was needed. The following pertinent information was used:

- Wall and coil wall thicknesses (0.375 in and 0.154 in (2-in OD Sch 40), respectively, with a corrosion allowance of 0.0625 inch) initially met the nominal values throughout tank.
- Coil welds were 100% radiographed.
- The tank is not expected to experience large evaporative losses since the tank purge is not expected to lead to a significant turnover in the vapor space.
- Coils would be the area of greatest concern since the wall thickness is thinner than the wall and the coils are used for heating, so the surface temperature would be greater than the desired process temperature.

Additionally, pertinent data from the current testing was also employed to evaluate the impact of the proposed acid digestions on the integrity of Tank 5.2 stainless steel surfaces. These data were:

- IGA is the primary mode of stainless steel corrosion during an acid digestion with subsequent grain dropping contributing to significant loss of material thickness on liquid-exposed surfaces.
- The greatest loss in thickness (~ 0.008 inch measured in base metal) was observed at the air/liquid interface followed by liquid-exposed surfaces. Vapor-exposed surfaces had minimal wall loss as based on corrosion rate.
- Condensation was maximized in the testing to minimize evaporative losses and maintain a steady or stagnant air/liquid interface.
- The neutral pH digestion simulated the historic H-Canyon caustic digestion.
- Repetitive exposure of stainless steel to the digestion solution leads to progressively greater corrosion as determined from the measured corrosion rates.
- Welds had greater depths of penetration than the base metal.

The current material condition of Tank 5.2 results from numerous caustic digestions and two acid digestions. Caustic digestions would not have corroded the coil and tanks walls or contributed to significant thickness loss. From the acid digestions, the liquid-exposed surface would have suffered IGA with the greatest depth of penetration at the air/liquid interface. Localized area on the liquid-exposed surface below the interface also would have depths of penetration due to grain drop out or

interdendritic attack at welds but less than at the interface. The air/liquid interface during the two proposed acid digestions will be lower than the previous acid digestions since less resin will be digested. This lower interface will cross some of the localized areas of grain drop out.

A conservative estimate for additional acid digestions is that the maximum test-measured wall loss (0.008 inch) will continue to occur at the current greatest loss of wall thickness whether at or below the previous interface. Since two digestions have occurred previously, the Tank 5.2 coil and wall thicknesses would have suffered a 0.016-inch loss. Doubling this value, for a safety margin, would give a wall loss of 0.032 inch. This value would account for the loss equivalent to the deepest depth of penetration on test coupons and allow for the impact of untested variables such as higher temperatures of coil surfaces. After the two proposed acid digestions, the total wall loss would be 0.064 inch, consuming the total corrosion allowance at localized spots, but not compromising the containment function of the tank. While Tank 5.2 is expected to withstand two additional acid digestions, a condition assessment of the tank, i.e. a visual examination or coil pressure testing, would provide valuable data on Tank 5.2 utility, especially at the end of any additional digestions.

## **5.0 Conclusions**

Continued usage of Tank 5.2 for acid resin digestion was recently questioned because of corrosion observed in a test apparatus during a prototype experiment of the process for measuring a hydrogen generation rate. The corrosion was postulated to be associated with the use of a chloride form of the resin which is not in use in the facility. An exploratory study was conducted to evaluate the impact of the chloride during acid digestion to assess the risk to Tank 5.2. The results from this study showed that intergranular attack is the prevalent form of corrosion whether chloride was present or not. The chloride may contribute to greater depths of penetration. The location of the air/liquid interface is the point of greatest degradation and would be expected to experience the greatest wall loss. Neutral pH digestion was found to cause minimal stainless steel corrosion. The historical Tank 5.2 caustic (neutral pH) digestion process is expected to have caused minimal loss of wall thickness. The past two acid digestions caused a wall loss of as much as 16 mils as based on measurements in this testing. Two additional acid digestions would contribute an additional 16 mils (32 mils total). An added safety margin of 32 mils is needed to account for parameters that were not part of this testing, yielding an estimated total wall loss of 64 mils. While this estimate would consume the corrosion allowance for Tank 5.2, the containment function of the tank is not expected to be compromised.

**Appendix A. Corrosion Assessment of Woodham HGR Test Equipment**

During an experiment modeling resin acid digestion to measure prototypical hydrogen generation rates the experimental apparatus was found to be severely corroded.<sup>8</sup> The corroded components included the 304L test vessel, the Alloy 800 heater rod, which failed due to penetration of the cladding, and the Inconel 600 sheathed thermocouple. The digestion was performed in nitric acid with potassium permanganate and 6 g of the resin. In the first experiment, the digestion solution was held at 70 °C for 15 hours after a 24-hour hold at room temperature. At the end of the digestion the solution was cooled down to approximately 50 °C and sodium hydroxide was added. This solution was held at 40 °C for 4 hours. The corrosion of the apparatus components was discovered upon opening the test vessel.

The three components were examined microscopically to perform a preliminary evaluation of the degradation and to determine plausible corrosion mechanisms. All three components were found to have intergranular attack (IGA) with areas of grain dropping. The IGA was on both liquid-exposed and vapor-exposed surfaces of the test vessel, which can be seen in Figure A-1. In this photograph, the graininess of the surfaces indicates the IGA observed on a microscopic level. This graininess can also be seen in Figure A-2 for the surfaces of the heater rod and thermocouple. While the IGA is over the entire surface for the 304L test vessel and Inconel 600 sheathed thermocouple, the IGA appears to be concentrated near the air/liquid interface for the Alloy 800 heating rod. One cause for IGA in stainless steels is very oxidizing conditions like those that occurred during this testing caused by the high molar nitric acid concentration, elevated temperature and presence of oxidizing species. These species are the added permanganate salt as well as  $\text{Cr}^{+6}$  which over time result from corrosion of the stainless steel.

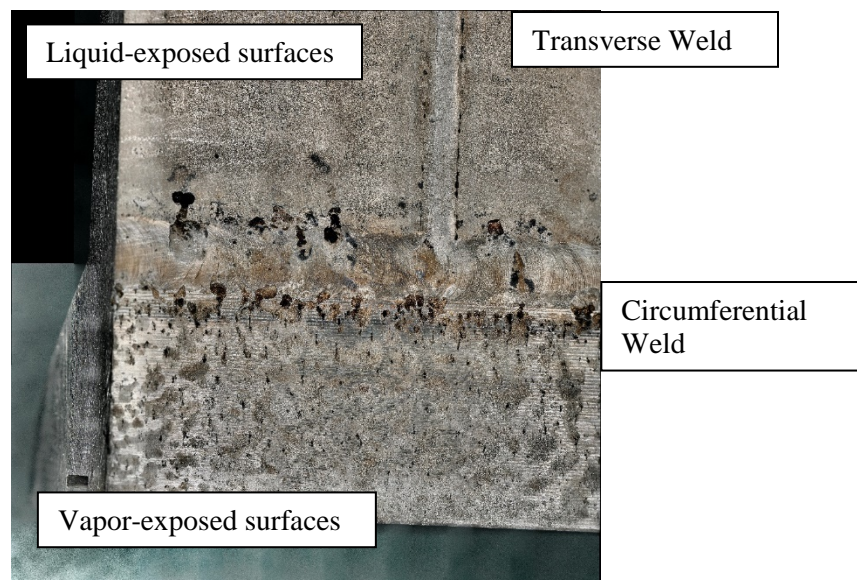


Figure A-1. 304L test vessel near joint of transverse and circumferential welds highlighting the IGA observed on all surfaces and the more severe corrosion in the circumferential weld, which was coincidental with the air/liquid interface

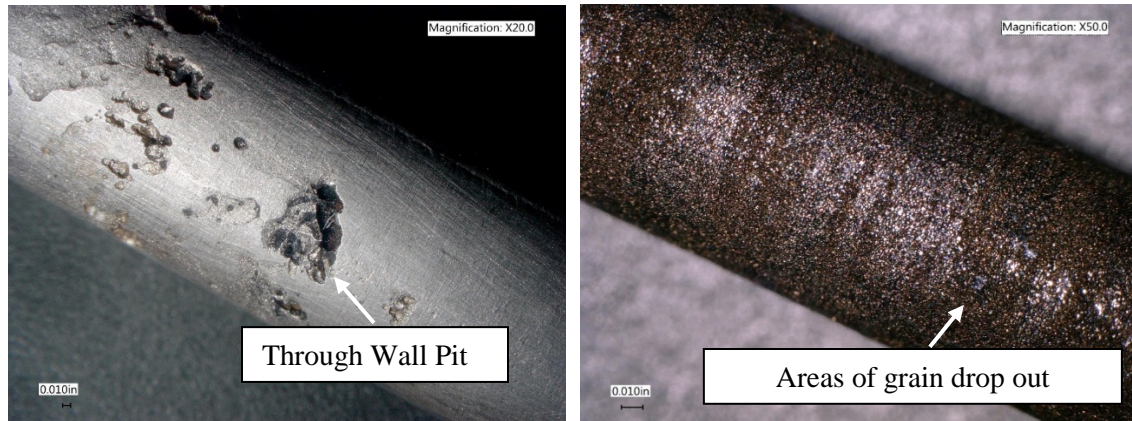


Figure A-2. Alloy 800 heater rod (left) and Inconel 600 sheathed thermocouple (right) showing surface graininess indicative of IGA; the failure spot of the heater rod is also shown

The test vessel and heater rod also had pit-like features. Their depths were measured in a couple locations and were found to be approximately 15 mils, which agreed with the results of a preliminary ultrasonic evaluation that was conducted (~ 20 mils). These features appeared to be concentrated at the air/liquid interface as shown in Figure A-1 for the test vessel and Figure A-2 for the heating rod. Suspect pitting was not apparent on the Inconel 600 sheathed thermocouple.

The actual mechanism for possible pitting was initially unclear since there was not a known source of chloride. Subsequent review of the HGR test conditions revealed that a chloride form resin was inadvertently used in the test. In heating situations, chlorides can concentrate due to evaporation. Since the suspect pitting appeared to be associated with the air/liquid interface, sufficient chloride concentration (>250 ug/g) may have occurred especially if floating resin particulate seen in Figure A-3 attached to material surfaces to form a crevice-type condition.



Figure A-3. Air/liquid interface initially (left) with the nitric acid and resin present and at the end of the test (right) after the NaOH has been added indicating the air/liquid interface was not stagnant during testing

The suspect pits may also be associated with aggressive IGA and subsequent grain dropping. The air/liquid interface was more oxidizing than immersed parts of the surface, highlighted by the

greater degradation along the circumferential weld than the transverse weld shown in Figure A-1. Two lines of pit-like features can be seen on each side of the circumferential weld, which appear to coincide with the different levels of the air/liquid interface shown in Figure A-3. For 304L, the deepest pit-like features are associated with the circumferential weld, which was coincidental with the air/liquid interface. Sensitization may also be a contributing factor along with the IGA and grain drop out. The requirements imposed for the welding of the vessel are not known. This rationale is not applicable to the heating rod, which failed by penetration of the cladding.

Some of the morphologies observed on the test vessel sidewall along the circumferential weld (Figure A-4) also indicate the possibility of stress corrosion cracking, which would require a high chloride concentration within a pit. The perpendicular linearity of degraded spots emanating from the weld and pit-like or crevice-like features are some indication. A cross section through the weld would be needed to confirm.



Figure A-4. Micrograph (200X) of circumferential and transverse weld joint showing linear indications of possible stress corrosion cracking (see arrows).

The apparent degree of corrosion is correlated to the Fe concentration and inversely correlated to the Ni/Cr concentration. The nominal compositions of the alloys are shown in Table A-1. The 304L test vessel suffered the worst corrosion on all surface while the Alloy 800 heater rod was concentrated at the air/liquid interface. The Inconel 600 sheathed thermocouple underwent IGA over the entire surface but did not fail in service as the heater rod. The ranking given for greatest to least corrosion is 304L > Alloy 800 > Inconel 600.

**Table A-1. Nominal Alloys Composition for Experimental Apparatus Components**

Material	Cr	Ni	Fe	Mn	Mo	Si	Other
304L	18-20	8-12	Bal	<2	--	<1	
Inconel 600	14-17	>72	6-10	<1	--	<0.5	
Alloy 800	19-23	30-35	>39.5	--	--	--	Al+Ti 0.15-0.6

**Distribution:**

*The standard distribution of all technical reports is:*

[timothy.brown@srnl.doe.gov](mailto:timothy.brown@srnl.doe.gov)  
[alex.cozzi@srnl.doe.gov](mailto:alex.cozzi@srnl.doe.gov)  
[david.crowley@srnl.doe.gov](mailto:david.crowley@srnl.doe.gov)  
[David.Dooley@srnl.doe.gov](mailto:David.Dooley@srnl.doe.gov)  
[a.fellinger@srnl.doe.gov](mailto:a.fellinger@srnl.doe.gov)  
[samuel.fink@srnl.doe.gov](mailto:samuel.fink@srnl.doe.gov)  
[nancy.halverson@srnl.doe.gov](mailto:nancy.halverson@srnl.doe.gov)  
[erich.hansen@srnl.doe.gov](mailto:erich.hansen@srnl.doe.gov)  
[connie.herman@srnl.doe.gov](mailto:connie.herman@srnl.doe.gov)  
[john.mayer@srnl.doe.gov](mailto:john.mayer@srnl.doe.gov)  
[daniel.mccabe@srnl.doe.gov](mailto:daniel.mccabe@srnl.doe.gov)  
[Gregg.Morgan@srnl.doe.gov](mailto:Gregg.Morgan@srnl.doe.gov)  
[frank.pennebaker@srnl.doe.gov](mailto:frank.pennebaker@srnl.doe.gov)  
[William.Ramsey@SRNL.DOE.gov](mailto:William.Ramsey@SRNL.DOE.gov)  
[luke.reid@srnl.doe.gov](mailto:luke.reid@srnl.doe.gov)  
[geoffrey.smoland@srnl.doe.gov](mailto:geoffrey.smoland@srnl.doe.gov)  
[michael.stone@srnl.doe.gov](mailto:michael.stone@srnl.doe.gov)  
[Boyd.Wiedenman@srnl.doe.gov](mailto:Boyd.Wiedenman@srnl.doe.gov)  
[bill.wilmarth@srnl.doe.gov](mailto:bill.wilmarth@srnl.doe.gov)

Records Administration (EDWS)

*For H-Canyon reports*

[timothy.tice@srs.gov](mailto:timothy.tice@srs.gov)  
[james.therrell@srs.gov](mailto:james.therrell@srs.gov)  
[kenneth.burrows@srs.gov](mailto:kenneth.burrows@srs.gov)  
[michael.lewczyk@srs.gov](mailto:michael.lewczyk@srs.gov)  
[john.lint@srs.gov](mailto:john.lint@srs.gov)  
[stephen.yano@srs.gov](mailto:stephen.yano@srs.gov)  
[jeffrey.schaade@srs.gov](mailto:jeffrey.schaade@srs.gov)  
[christine.hadden@srs.gov](mailto:christine.hadden@srs.gov)  
[Richard.Burns@srs.gov](mailto:Richard.Burns@srs.gov)

*Other SRNL*

[Roderick.Fuentes@srnl.doe.gov](mailto:Roderick.Fuentes@srnl.doe.gov)  
[jonathan.duffey@srnl.doe.gov](mailto:jonathan.duffey@srnl.doe.gov)  
[Tara.Smith@srnl.doe.gov](mailto:Tara.Smith@srnl.doe.gov)  
[Wesley.Woodham@srnl.doe.gov](mailto:Wesley.Woodham@srnl.doe.gov)  
[chris.martino@srnl.doe.gov](mailto:chris.martino@srnl.doe.gov)  
[john.mickalonis@srnl.doe.gov](mailto:john.mickalonis@srnl.doe.gov)  
[bruce.wiersma@srnl.doe.gov](mailto:bruce.wiersma@srnl.doe.gov)  
[kristine.zeigler@srnl.doe.gov](mailto:kristine.zeigler@srnl.doe.gov)